SPIE.SPOTLIGHT

Biofunctionalized Photoelectric Transducers for Sensing and Actuation

George K. Knopf and
Khaled Al-Aribe

Biofunctionalized Photoelectric Transducers for Sensing and Actuation

by George K. Knopf and Khaled M. Al-Aribe

doi: http://dx.doi.org/10.1117/3.2283084
PDF ISBN: 9781510613669
epub ISBN: 9781510613676
mobi ISBN: 9781510613683

Published by

SPIE Press
P.O. Box 10
Bellingham, Washington 98227-0010 USA
Phone: +1 360.676.3290
Fax: +1 360.647.1445
Email: Books@spie.org
Web: http://spie.org

Spotlight vol. SL31
Last updated: 28 July 2017

SPIE.

Table of Contents

SPIE Spotlight Series

Welcome to SPIE Spotlight eBooks! This series of tutorials is designed to educate readers about a wide range of topics in optics and photonics. I like to think that these books address subjects that are too broad for journal articles but too concise for textbooks. We hope you enjoy this eBook, and we encourage you to submit your ideas for future Spotlights online.

Robert D. Fiete, *Series Editor*
Harris Corp.

Editorial Board

Preface

Over the past several decades, researchers around the world have exploited a light-responsive protein called bacteriorhodopsin (bR) to create thin organic films that can function as photocells and photoelectric biotransducers. From an engineering perspective, the proton transfer mechanisms of bR purple membranes have been used to develop various optoelectronic devices. This Spotlight describes the functional molecular behavior of bacteriorhodopsin, techniques for molecular self-assembly, and applications for bioelectronic sensing and microactuation.

1 Introduction

Over the past several decades, researchers around the world have exploited a light-responsive protein called "bacteriorhodopsin" (bR) to create a variety of thin organic films that can function as photocells, photoelectric biotransducers, and light-driven proton pumps. In nature, the bR molecules are found in the cellular membranes of the salt-marsh archaebacteria *Halobacterium salinarium* and are used to generate the potential difference necessary for synthesizing adenosine triphosphate (ATP) from adenosine diphosphate (ADP). Under oxygen-limited conditions, the *Halobacterium* cell grows planar purple membrane (PM) patches in the form of a hexagonal 2-D crystalline lattice of bR trimers. When exposed to visible light beams, each bR molecule acts as a simple proton pump, which transports hydrogen ions from the cytoplasmic to the extracellular side through a transmembrane ion channel that connects both sides of the membrane. The crystalline structure is the basis of the bR material's chemical and thermal stability.

From an engineering perspective, the proton transfer mechanisms of bR PMs have been used to develop a number of different optoelectronic devices. For example, bR-coated silica microcavities and microspheres have been used to perform all-optical switching in the near-infrared spectrum. Additionally, the bR PMs have been deposited and immobilized on optically transparent indium tin oxide (ITO) electrodes to construct bioelectronic photodetector arrays that respond to light intensity, movement of light patterns, and color (i.e., spectral sensitivity). The proton transfer mechanisms of bR PMs have also been used to fabricate photoelectric biotransducers for activating ionic gel actuators in microfluidic chips. In these devices, the flow of ions from the photon-activated bR changes the pH value of the ionic solution that surrounds the hydrogel microactuator or microvalve. Once the pH of the gel's solution is shifted to the phase transition point pKa, the chargeable pendant groups of the polymeric network undergo a measureable geometric transition. However, the fabrication of efficient thin photoelectric layers and their directional proton pumps requires the molecular recognition of the extracellular side of the bR proton pumps and effective immobilization of the PM monolayer on the functionalized substrate.

This Spotlight briefly summarizes the molecular behavior of bR, introduces thin-film fabrication techniques with an emphasis on molecular self-assembly, and describes its application to all-optical switches, bioelectronic photosensing, and light-driven microactuation. The primary goal of this book is to advance the understanding of photosensitive bioelectronics technology and provide an inspiration for the next generation of scientists and engineers to develop innovative solutions far beyond anything that we can imagine today. The opportunities for product innovation, by applying the basic principles of light-responsive bR films, are illustrated by several novel systems.

2 Bacteriorhodopsin: Nature's Solar Cells

Photoelectric films are an essential component of a light-driven system that exploits solar radiation or the photon energy inherent in a focused light beam (e.g., laser). One organic material that has been extensively studied for creating photocells and a diverse variety of optoelectronic devices is bR, a light-sensitive protein found in the salt-marsh archaebacteria *H. salinarium*. In nature, these bR protein molecules employ the sun's energy to transport hydrogen (H^+) ions across the *Halobacterium* cell membrane, thereby generating the potential difference necessary for synthesizing ATP from ADP.[1–3]

The synthesis of ATP from ADP is required for bacterial cell activities.[1,2] Biologically, the ATP is known to be the energy transfer agent that diffuses in the cell to energize its cellular molecular processes and cell movements.[4] However, this photosynthesis in bR is fundamentally different from the chlorophyll-mediated photosynthesis found in plants. Energy conversion in the latter case starts with electron charge separation, whereas in bR the process of conversion of light energy into a usable form of energy starts by pumping hydrogen ions across the membrane to produce an electrochemical potential.[5,6]

Under oxygen-limited conditions, the *Halobacterium* cell grows planar PM patches in the form of a hexagonal 2-D crystalline lattice of bR trimers. When exposed to light from the visible spectrum (390 to 700 nm), each bR molecule acts as a simple proton pump, which transports H^+ ions from the cytoplasmic to the extracellular side through a transmembrane ion channel that connects both sides of the membrane (Fig. 1). The crystalline structure is the source of the bR material's chemical and thermal stability. The PM has been shown to be stable

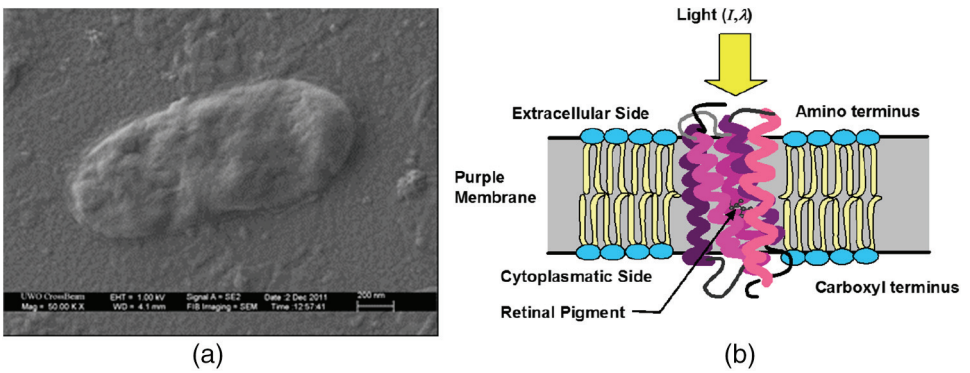

Figure 1 (a) SEM photograph of a bR PM fragment, and (b) an illustration of a *H. salinarium* biological cell showing the structure of bR PM patches. The incident light is given as intensity (I) and wavelength (λ). The bR monomer is a retinal pigment material that penetrates through the cell membrane from the cytoplasmic side (inside) to the extracellular side (outside) of the membrane.

for several years while being exposed to prolonged periods of sunlight. The PM even preserves its photochemical and photoelectric activity under dry conditions, and can withstand relatively high temperatures of up to 140°C.[2]

The PM fragments are bR proteins composed of linear pigment retinal bounded between seven amino helices arranged inside a lipid layer.[7,8] A closer look at the PMs reveals that these patches are isolated in irregular ~5-nm-thick sheets.[9,10] Each PM fragment is composed of 75% bR and 25% lipids in hexagonal symmetry.[2] The bR molecule contains a functional molecule, called a "retinal," which gives the bR PM its purple color.

2.1 Photocycle of bacteriorhodopsin molecules

The retinal of the bR proton pump is a natural chromophore that exists only in one of two configurations: all-*trans* and 13-*cis*.[11] In the absence of light, known as the "dark-adapted state," the bR molecules contain a mixture of these two retinal configurations. The pumping of protons (H^+ ions) across the cellular membrane does not occur in the dark-adapted bR. Once the bR molecules are exposed to light radiation, the molecules that are in the 13-*cis* configuration ground their state to be at the all-*trans* retinal configuration. This is called the "light-adapted state" and is considered as the starting point of the photocycle. During the transition to the light-adapted state, the retinal undergoes an isomerization process around the C13═C14 double bond to transform the retinal configuration from all-*trans* to the 13-*cis* configuration,[12] as shown in Fig. 2. The retinal isomerization is followed by proton transport from the cytoplasmic to the extracellular side of the membrane, which is interpreted as converting the incident light energy into chemical energy.[13] The proton pumping process is accompanied by a thermal structure-relaxing photocycle with several intermediate states.

Prior studies[14,15] have shown that the kinetics of the photocycle depend on the level of humidity in the bR sample. The photocycle and proton transfer kinetics of

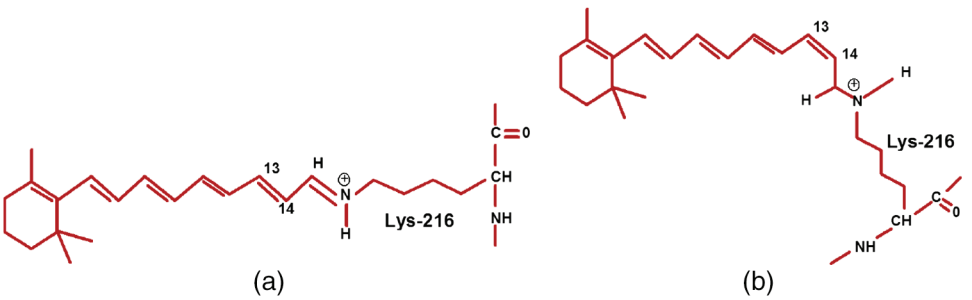

Figure 2 Photoisomerization of the bR retinal from (a) all-*trans* to (b) 13-*cis* configuration in bR.[12] The retinal has a covalent bond with Lys-216 via a protonated Schiff base. When absorbing a photon, the retinal isomerizes around the C13═C14 bond.

wet (or aqueous) bR will differ from dried bR because of dehydration.[15–19] In the bulk aqueous form [Fig. 3(a)], the bR molecules act as a light-driven proton pump. The absorption of a photon by the bR molecule initiates the isomerization of retinal from all-*trans* to 13-*cis* conformation, followed by proton transport across the cell membrane. The PM proton transfer starts with the release of a hydrogen ion (H^+) during the $L_{550} \rightarrow M_{412}$ transition and ends with an ion uptake during the $M_{412} \rightarrow N_{560}$ transition. Note that the subscripts identify the peak wavelengths of light responsible for the transition. The light-induced intermediate states of the photocycle correspond to activation, proton dissociation, proton translocation, proton association, and relaxation.

When exposed to visible light, the bR molecules return to the ground state B_{570}. This step is considered as the start point of the photocycle. The photocycle consists of photo-driven thermal intermediates with distinct photoabsorption maxima. Fundamentally, the photocycle's intermediates are wavelength (λ) driven transitions, where each intermediate can proceed by thermal relaxation to the next state or switch back to the ground state B_{570}, based on the received photoexcitation. All of the intermediates are before the proton release and after the proton uptake. The transition of the bR that occurs between releasing a proton and uptaking another proton is considered as an irreversible transition, where the nitrogen atom in the Schiff base becomes no longer accessible to the extracellular side of the proton way half-channel, which then opens the cytoplasmic side of the half-channel and closes the extracellular half.

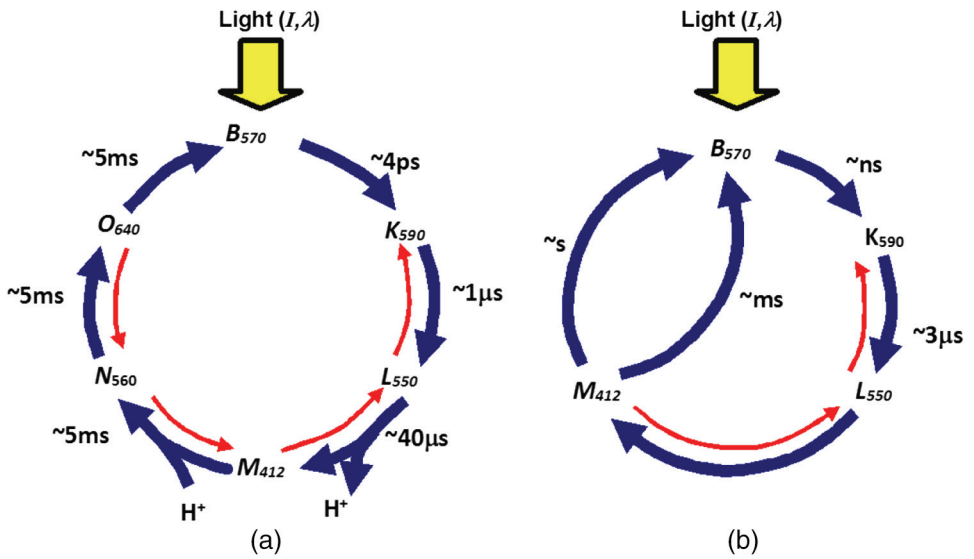

Figure 3 The photochemical cycles of (a) aqueous and (b) dried forms of bR when exposed to visible light (I, λ). The subscripts refer to the peak wavelength for the identified intermediate.

The sequence of the proton release–uptake is a pH-based process, such that when pH $\geq$ 7.0, the proton release precedes the proton uptake. In contrast, when the pH < 7.0, the proton uptake precedes the proton.[20] These simultaneous structural rearrangements are considered to be the origin of the vectorial proton transport through the bR protein. In the wild-type bR proton pump, a complete photocycle needs ~10 ms.[21]

However, when the humidity level in the bR film falls below 90%, the later N_{560} and O_{640} intermediates are no longer observed, and fewer protons are transferred across the PM.[22] As shown in Fig. 3(b), only the K_{590}, L_{550}, and M_{412} intermediates of the dry bR are involved in the photochemical cycle. The dry bR protein returns to its ground state (B_{570}) through several paths, each with a different lifetime.[7] Furthermore, the only available ions for dry bR film are those enclosed within the structure of the bR PM proton pumps (retinal ions).

Both aqueous and dried bR PMs have the same spectral absorbance, as shown in Fig. 4, and exhibit a peak photoexcitation response at 568 nm. The optical absorbance at a given wavelength is related to the ratio of light intensity transmitted through a sample to the original incident light intensity.

2.2 Proton pumping mechanism in thin bacteriorhodopsin films

bR is the only protein present in the plasma membrane of *H. salinarium*. Under anaerobic conditions, the cell membrane grows PM patches in the form of a hexagonal 2-D crystalline lattice of bR trimers. These PM patches consist of a 10:1 molar ratio of lipids to bR.[2,6] The bR molecules convert sunlight into chemical energy by transporting protons from the cytoplasm to the cell exterior. In addition, PM does not allow passive diffusion of protons back into the cell. The bR

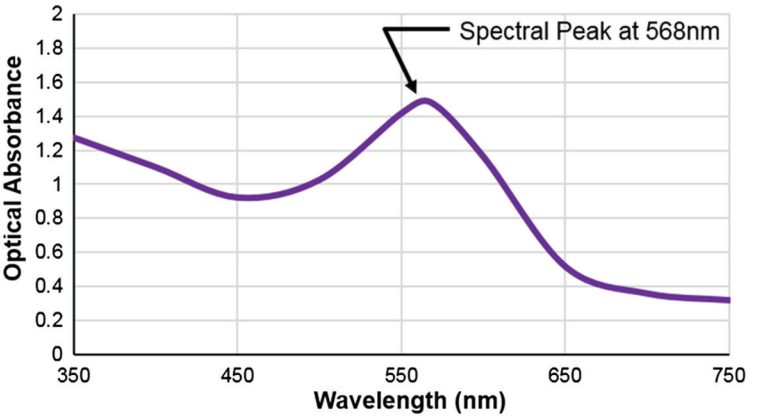

Figure 4 Measured optical absorbance of bR over the visible spectrum using a μQuant Microplate Spectrophotometer from Bio-Tek Instruments (Western University).

molecule is a type of retinal–protein complex and consists of two parts: a protein molecule (i.e., bR) and a retinal molecule (vitamin A aldehyde).

Each bR molecule consists of 248 amino acids structured in seven-helix receptors (**A** to **G**) formed around a molecular transmembrane channel.[2,23] Each helix is attached to either side of the cell membrane. Inside the seven-helix bundle structure, there is a light-responsive pigment called a retinal. One end of the retinal is coupled to the nitrogen atom of the helix **G** at its lysine residue. The other end of the retinal is angled in the transmembrane channel. The amino-acid-based chains of the bR helices form polypeptide loops that work as a binding pocket that keeps the retinal in its coordinates within the transmembrane channel. This molecular arrangement is the key factor to allow the retinal to be accessible by the incident light and enable trapping the received photons within the transmembrane channel. The energies of the trapped photons drive hydrogen ions from the intercellular to the extracellular side of the PM.

The proton pumping process consists of a series of molecular events that are associated with reversible structural deformations.[8] These structural deformations are called bR intermediates *K*, *L*, *M*, *N*, and *O* (Fig. 3). In addition to the induced structural deformations, each intermediate provides the structure with different colors. These intermediates are extensively studied using electron cryomicroscopy[23] and x-ray crystallography of microcrystals.[24]

The pumping mechanism starts at the ground state when light hits the protein's retinal, passing through structural deformations, and ends by returning to the ground configuration. This series of events can be categorized in the four major intermediates. Once a light beam hits the retinal, it undergoes a conformation change from the all-*trans* to the 13-*cis* in 1 ps to generate the *K* intermediate. During this intermediate, one end of the retinal molecule rotates about the carbon double bond, which displaces part of the pigment to the protein's scaffold. These movements energize the hydrogen ion, which is attached to the nitrogen to move in 50 μs to aspartate 85, through tyrosine 89, or to aspartate 212 and firmly bind a water molecule to generate the intermediate *L*.[8] One factor that motivates the proton to move is the elastic deformation of helix **C**, which displaces the side of aspartate 85 toward the nitrogen.[25]

Once the proton starts moving, the retinal's color changes from pink to yellow, and its molecular chain becomes straighter. Following these structural changes, the nitrogen atom moves upward to be closer to the intercellular side by 0.7 to 1.0 Å by displacing a number of residues of helix **F**.[26] The displacement of helix **F** residues generates lever-like momentum on the upper part of helix **F**. This momentum swings the helix **F** outward by 3.5 Å to reach the *M* intermediate, during which the helix **G** returns partly to its original position. During these movements, the retinal receives a proton from aspartate 96 and bends again to the original angled position, reaching intermediate *N*. During the intermediate's transition from *N* to *O*, the hydrogen ion of the aspartate 85 moves to the chain's

hydrogen bonds with water molecules in the lower part of the channel.[27] The pumped proton is allowed to depart from the membrane by the displacement of the arginine 82 toward the bottom of the membrane. Finally, the retinal reconfigures its conformation to all-transform, and the helices **F** and **G** return to their ground position. This sequence of events on a single bR molecule results in pumping one proton, with the capability to pump up to 100 protons/s.

2.3 Photoelectric properties of bacteriorhodopsin films

The photoelectric response behavior of aqueous and dried bR that depends upon the light–bR interactions and the charge dynamics within the bR protein can be directly related to the intermediate kinetics of the photocycle. When bR receives light, it starts the charge translocation process and the sub-sequential structure deformations needed to generate charge gradients.[13] This charge activity can be detected by monitoring the potential difference across the bR material. The existence of a measureable voltage difference and the temporary changes in both the polarity and amplitude can be directly related to the proton transfer across the PM patches.

The photoelectric response of bR proton pumps and dried bR films originates from two effects that occur during the photocycle.[28] The first effect is the proton translocation across the PM arising from the pumping action from the intracellular side to the extracellular side. This effect requires the presence of water and is observed as a DC photocurrent through the bR material. The second effect is the charge displacement and recombination within the bR molecule. This effect is less sensitive to humidity or moisture content. It is, however, essential for the photoelectric behavior of dried bR films and is observed as an AC photoresponse signal.

When exposed to light radiation, appropriately oriented PMs will generate a photoelectric signal that contains three major components with different lifetimes. The internal charge dynamics, proton dynamics, and nonproton ion dynamics contribute to these photoelectric components. The fastest component is in the direction opposite to the proton movement and exhibits a rise time of <100 ps.[29] The remaining two photoelectric components are in the same direction as the proton transfer and occur in μs and ms ranges.[30]

Theoretically, the photocycle lifetimes should coincide with the photoelectric components. However, the lifetimes of the PM photocycle components are not in full agreement with the detected responses.[31] In addition to distortions introduced to the photoresponse waveform by the measuring instruments, these differences may also arise because of the fabrication techniques used to orientate and adsorb the PMs on the electrode's surface. Another source of inconsistencies in the observed photo signals can be attributed to the surrounding environment that may contain high salt concentrations.

3 Building Thin Photoelectric Monolayers and Films

To develop viable light-driven microelectromechanical systems (MEMS) and microfluidic systems using bR material, it is necessary to properly immobilize the bR on nonporous electrically conductive surfaces for constructing photoelectric devices or on porous membranes for fabricating pH gradient proton pumps. Common immobilization techniques include electric field sedimentation (EFS), Langmuir–Blodgett (LB), electrostatic layer-by-layer adsorption, antigen–antibody molecular recognition, and molecular self-assembly.[31–33]

Although the measured photoelectric behavior exhibited by the engineered bR device will be the result of large numbers of PM proton pumps, efficient photon to ion flow and charge separation requires consistent orientation of the PM patches on the conductive substrate or membrane. It is important to realize that the resultant signal arising from two bR pumps with opposite orientation is zero.[34] Consequently, a thin-film fabrication technique that produces PM patches with a mixture of both cytoplasmic and extracellular sides being adsorbed on the same electrode will result in a significantly weakened photoelectric response.

To properly exploit the photoresponsive bR material in an engineered system, it is necessary to control how the bR proton pumps are adsorbed onto the substrate. Orientation specificity can be achieved by using either the antigen–antibody immobilization method,[35] the genetically engineered bR protein,[34] or the biotin-labeling technique.[36–38] Although the antigen–antibody technique produces satisfactory orientation of the bR, the process is very lengthy because it is necessary to synthesize antigens, monoclonal antibodies, and biantibodies. On the other hand, using genetically modified bR protein might not be very convenient for designers without knowing the detailed characteristics of the generated product. Producing the genetically engineered PMs also necessitates genetic modifications to the protein in order for the PM to be connected to the gold substrate via thiols. In contrast, the biotinylation technique described in Section 3.2 uses only one reactive residue that is located at the extracellular side of bR, and it can be accessed at a specific pH, making biotin labeling a highly repeatable and reproducible process at the molecular level.

3.1 Immobilizing organic materials on substrates

Two challenges must be addressed prior to incorporating biomaterials into practical devices: patterning biomaterials and interfacing them with conventional systems. These tasks require immobilization techniques that can appropriately orient the protein molecules and prevent them from denaturing. Thin films are currently considered to be the most practical structures for photosensitive materials over that of the bulk state due to their improved photoelectric performance and functionality. Thin films also allow straightforward configurations that permit the biological components to interface with microelectronic systems. Three methods often used to assemble bR thin films on solid substrates are described in this section.

The LB deposition technique is a common method used to create highly ordered and ultrathin films of organic molecules that have amphiphilic properties.[39] In this method, amphiphilic molecules are spread across the water surface in a trough, compressed by a barrier, and transferred to a solid substrate by horizontal or vertical dipping techniques. Multilayered films are formed by applying this process repeatedly. PMs are oriented with their cytoplasmic sides toward the water phase and the extracellular side directed into the air, as the cytoplasmic side of PM is more hydrophilic than the extracellular side (Fig. 5).

To improve PM orientation in LB films, an electric field can be applied across the air–water interface. Even though it is possible to prepare oriented LB films that have a high degree of bR orientation and good optical response, the LB technique must be carefully prepared because PM fragments are liable to denature in most organic solvents. The preparation of multilayered bR films becomes very complex due to the electrostatic interaction between each layer and the other layers in the range of its electrostatic interaction. Moreover, it is a time-consuming process because the LB procedure must be repeated many times under controlled conditions, thus limiting its use in practical device fabrication.

Another approach to fabricating thin bR films with oppositely charged species onto a solid substrate is the electrostatic layer-by-layer (ELBL) adsorption technique. The ELBL technique is a versatile and effective method of assembling oppositely charged species onto solid substrates. This technique is based on strong electrostatic interactions between oppositely charged polyelectrolytes.[32] PM patches have asymmetrically charged surfaces, making PM particularly suitable for layering using the LBL method. Figure 6 shows a schematic diagram representing the poly(dimethyldiallyl)ammonium chloride (PDAC)/PM multilayers in these assemblies. Because the cytoplasmic side of PM exhibits more negative

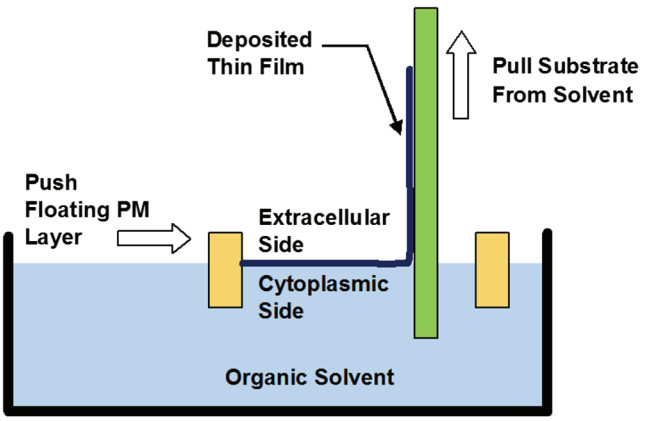

Figure 5 Preparation of a bR film by the LB deposition technique. Because the cytoplasmic side of PM is more hydrophilic than the extracellular side, the former has a preferred orientation facing into the water.

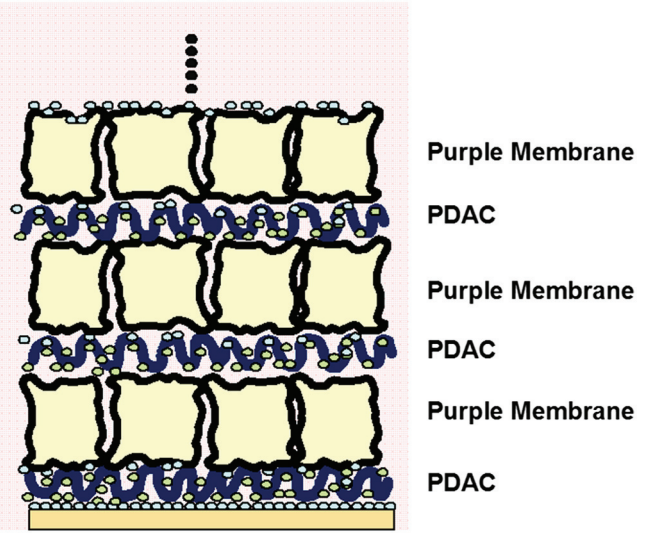

Figure 6 Schematic diagram of multiple PDAC/PM layers as fabricated by the ELBL adsorption technique. (Adapted from Ref. 32.)

charges than the extracellular side at pH values above 5, it is believed that the cytoplasmic side preferably attaches to the PDAC layers during the electrostatic adsorption process. This approach is readily applicable to a variety of other charged molecules, such as conducting polymers, nanoparticles, enzymes, and proteins; this indicates the potential for interfacing these molecules with bR to either enhance bR properties or add additional functionality to optoelectronic applications. However, continuous and homogeneous multilayer film formation cannot be obtained if the complete charged obstacle layers are not guaranteed.

The EFS technique is another common film fabrication method that provides a simple and effective means of achieving a high degree of bR orientation during film formation. When the PM suspension is placed between two parallel electrodes within an applied electric field, PM patches orient, transport, and deposit onto the anode (Fig. 7). It has been reported that bR films fabricated by EFS produce higher photocurrents compared to many of the other methods.[40] EFS is most often used because the process retains the functionality of the chromophore in the molecules.[1,14,41–43] The EFS utilizes the difference in negative charge density between the opposite sides of the PM to generate a dipole moment that is specifically directed from the cytoplasmic side to the extracellular side. However, this method of film fabrication is problematic because both sides of the protein are negatively charged with only a small measurable difference (−1.8 charge/bR: −2.5 charge/bR at pH 6.6),[32] making it nearly impossible to properly specify orientation of the PM patches. Consequently, the EFS immobilization technique attracts both

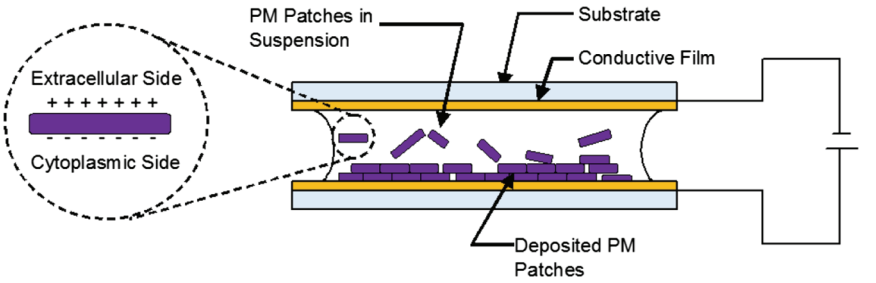

Figure 7 Fabrication of oriented bR films by the EFS technique. PM patches transport onto the anode due to its more negatively charged cytoplasmic side.

sides of the PM patches with no specificity regarding whether it is on the cytoplasmic or extracellular side.

Furthermore, the thin dry films fabricated using the EFS technique are often characterized by a surface roughness of ~200 nm,[42] and film thicknesses between 10 and 150 μm.[1,42,43] The relatively thick film indicates that thousands of bR layers are stacked on the cathode surface. The reported large surface roughness suggests that not all PM patches in the final layer of the film will make direct contact with the opposite electrode during operation, and thus the signal will be weaker than expected. Although thinner bR films can be fabricated using the LB technique, published studies[32,44] have shown that the PM patches that compose the thin film exhibit random directional orientation.

3.2 Immobilization by molecular self-assembly

To properly exploit the bR proton-pumping functionality in an engineered system, it is important to control how the bR proton pumps are deposited onto the substrate. Orientation specificity can be accomplished using the antigen–antibody immobilization technique,[35] the genetically engineered bR proton pumps zero,[34] or the biotin-labeling method.[33] Even though the antigen–antibody method can generate satisfactory orientation of the bR, the process is very lengthy as it involves the synthesis of antigens, monoclonal antibodies, and biantibodies. On the other hand, the use of genetically engineered bR protein may not be very convenient for engineers to use it without knowing the detailed characteristics of the created bR. Producing the genetically modified PMs also involves genetic modifications to the bR protein in order for the PM to be adsorbed on the gold substrate via thiols. In contrast, the biotinylation and streptavidin molecular recognition technique uses only one reactive residue that is found in the extracellular side of the bR proton pump, where it is accessible at a specific pH.

A biotin labeling and streptavidin molecular recognition technique can also be used to attach uniformly oriented PM patches to the substrates. The biotin enables

the extracellular side of the bR PMs to be accurately labeled and properly oriented to permit the efficient transport of ions in only one direction across the transducer layer (Fig. 8). This ensures the efficient transport of ions across the PMs. During the biochemical immobilization process, the biotinylated alkyl thiols modify the Au surface using HS terminals of the thiols and affix the labeled bR to the functionalized surface using streptavidin–biotin interactions.

The biotin labeling and streptavidin recognition technique employs selective molecular labeling, recognition, and adsorption to enable the self-assembly of proteins and other biological material at very specific sites on the sensing surface. This highly selective immobilization technique has been used to build a variety of integrated biosensors for detecting *Escherichia coli* bacteria[45] and bacteriophages,[46] as well as to develop molecular switches.[47] The fabrication of this thin photoelectric layer requires molecular recognition of the extracellular side of the bR proton pumps using biotin[36] and then building a self-assembled thiol monolayer on the gold substrate. The spontaneous adsorption of the labeled bR proteins on the thiol monolayer is achieved by a streptavidin molecular recognition and binding technique.

Gold (Au) surfaces are characterized by their high affinity for thiol adsorption, thereby enabling permanent bonds to be formed between the HS terminal of the thiols and the Au surface.[48] One of the most reliable methods to build self-assembled monolayers activates the substrate with biotinylated thiols. The thiols are chemical chains that have a HS terminal, which is characterized by its high affinity to gold,[48] and another terminal that can be permanently activated with biotin. The self-assembly of the labeled bR proteins on the thiol monolayer is accomplished by a streptavidin molecular recognition and binding capabilities. The biotin activation of the thiol layer makes the adsorption of the biotinylated bR proton pumps possible by using a streptavidin matrix.

An important feature of the molecular self-assembly technique is that very thin photosensitive "layers" can be deposited on the substrate. Direct experimental measurement of the photosensitive layer's thickness is difficult because the

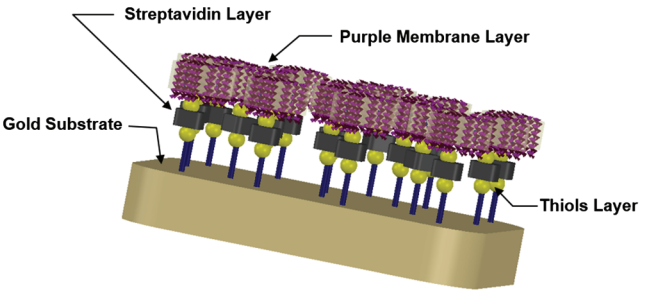

Figure 8 Illustration of the self-organized and self-assembled photoelectric dry layer on gold (Au) substrate.

observed values are dependent on the precision and sensitivity of the instrument. Because the dimensions of the constituent components of the self-assembled monolayer are known, it is also possible to theoretically compute the thickness of the photosensitive layer. The individual PMs have a thickness of 5 nm,[2] the streptavidin is 5.8-nm thick,[49] and the biotinylated thiols form a 2.7-nm thick monolayer. Therefore, the overall thickness of the photosensitive layer in its aqueous phase is calculated to be around 13.5 nm. This theoretical analysis validates the AFM measurements, which showed 12.33 nm for the full structure.[33] The small difference between the measured thicknesses of the dry bR and the calculated thickness of the aqueous bR is believed to arise from the reduction in water content during the drying process of the actual bR film. The photoelectric bR structure is an ultrathin layer (~13 nm) of oriented PM patches self-assembled on an Au-coated functionalized substrate.[33]

Ideally, the bR immobilization process would produce an ultrathin layer of PM that covers the entire Au substrate. However, experimental observations confirm that molecular self-assembly fabrication techniques do not produce a continuous uniform monolayer of closely arranged membranes.[34,50] The sporadic distribution of PM fragments on the substrate may be the result of small electrostatic repulsive forces between the constituent fragments.[2,32] These forces likely arise because individual fragments have a net negative charge above the PM's isoelectric point.[2,32]

The surface coverage on the nonporous and porous substrates was examined by using focused ion beam scanning electron microscopy (FIB-SEM; Fig. 9). The substrate surface topology (i.e., roughness), concentration of thiols, concentration of the streptavidin, and concentration of the biotinylated PMs play critical roles in determining the final distribution of PMs on the gold substrate.

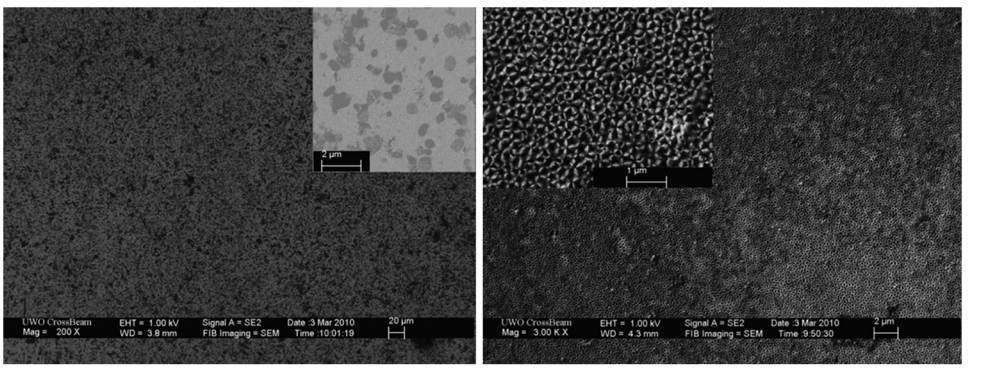

(a) (b)

Figure 9 SEM photographs of the self-assembled bR film on (a) nonporous and (b) porous Au-coated substrates. Enlarged areas are shown in upper corners (Western University).

4 Organic Photovoltaic Cells

One of the most common and practical energy-harvesting technologies that convert streams of photons into usable electricity is photovoltaic (PV) cells. Recent advances in materials science and engineering have enabled these light-to-electricity transducers to be fabricated from a large variety of solid-state semiconductors, photosensitive organic dyes, and photoactive proteins. Typically, a solid-state PV device consists of two parallel thin silicon (Si) semiconductor wafers that promote the formation of an electric field. As the light strikes the Si-based PV cell, the semiconductors exhibit a photoelectric effect that causes the silicon material to absorb the photons and release electrons producing an electric current. The more common silicon PV cells have a single-junction configuration that requires the photon energy to be equal to, or greater than, the bandgap of the absorbing material. This implies that single-junction PV cells can only produce electricity over limited ranges of the electromagnetic spectrum. Lower-energy photons from the light source are not used and, therefore, cannot be converted into useful electricity. Higher total conversion efficiency can be realized by using multijunction PV cells. The typical multijunction PV cell is composed of a stack of single-junction cells with a descending order of bandgap.

In contrast, PV cells developed from photosensitive organic dyes and photoactive proteins have gained popularity in the past decade because these devices are often cheaper and require far less energy during manufacturing. One promising alternative to the Si-based PV cell is a dye-sensitized solar cell (DSSC). Typically, a DSSC comprises a photoactive dye, a mesoporous (pore size 2 to 50 nm) nanocrystalline semiconductor layer coated on a transparent conducting oxide substrate (i.e., anode), a liquid electrolyte, and a Pt-coated transparent conducting oxide substrate (i.e., cathode).[51] When excited by a light source, the excited dye molecules inject electrons into the conduction band of the nanocrystalline semiconductor. The electrons are collected by the anode and flow through the outer circuit to the Pt-coated cathode. The molecules of the selected dye will play a critical role in the functional performance of the PV cell. The greatest efficiency for power conversion has been 11% using ruthenium bipyridine derivatives.[52,53] Unfortunately, these scarce synthetic organic and inorganic dyes can cause problems during mass production because of toxic effects on the environment.[51]

Biomaterials, such as natural dyes extracted from plants,[54] living photosynthetic micro-organisms,[55] proteins with solid-state electronics,[56,57] and cyanobacteria cells,[58] have also been investigated as photosensitive materials for making biosensitized solar cells (BSSCs). One of the more studied BSSC materials is the bR protein.

Researchers have also exploited the proton transfer mechanisms of bR PMs to develop a variety of engineered bR-PV cells for different applications. The light-responsive behavior has been used to create novel bioelectronic imaging

arrays[1,59–61] and color sensors.[60] The bR-based photoelectric structures can also be used to induce volumetric phase transitions in pH-sensitive polymer gels.[10,33,62] The basic design of simple PV cells that exploit photosensitive dry and aqueous (wet) bR thin films for generating small voltages is shown in this chapter. Although a variety of immobilization techniques can be used to create the photoresponsive films, the molecular self-assembly method is preferred in order to achieve thin films with properly orientated PM patches.

4.1 Dry bacteriorhodopsin photovoltaic cells

Once built on the Au substrate, a functional dried bR-PV photocell can be created by placing an optically transparent ITO contact glass plate on the ultrathin dry film [Fig. 10(a)]. The gold and ITO surfaces act as microelectrodes that permit this simple sandwich structure to form a closed electronic circuit. The photocell constructed from bR PMs can be modeled by a simple equivalent electronic circuit,[1,42,63] as shown in Fig. 10(b).

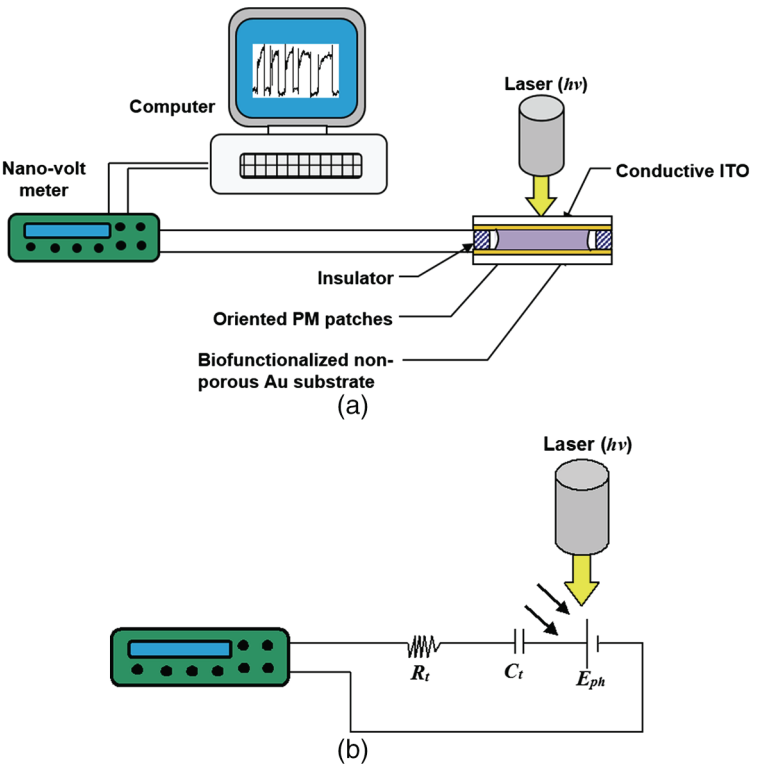

Figure 10 (a) Experimental apparatus and (b) equivalent electronic circuit used to test the photoelectric properties of the dry bR-PV cell.

The photovoltage source E_{ph} is formed by the light-responsive bR monolayer. The total capacitance C_t represents the combined effect of the chemical capacitance arising from the charge displacement process and the biological capacitance of the PMs. The total resistance is a result of the PM resistance and the contact resistance between the bR monolayer and the electrodes. It is important to note that the space between the microelectrodes is determined by the physical flatness of the electrodes and the thickness of the bR monolayer architecture (~13 nm). An in-depth discussion about mathematically modeling the bR behavior and developing a more detailed electronic circuit model can be found in the work by Wang,[64] Xu,[42] and Wang et al.[18]

Al-Aribe et al.[33] used an 18-mW, 568-nm Melles Griot argon ion laser to provide a controlled light source to the bR-PV cell. The 568-nm light source was used in these experiments because the peak photoexcitation of bR occurs at this wavelength.[2] The voltage differences were measured using an Agilent 34420A nanovolt/micro-ohm meter. The space between the microelectrodes is determined by the physical flatness of the electrodes and the thickness of the bR monolayer architecture. No additional signal processing or amplification was performed in an effort to minimize distortions of the experimental readings.

To investigate the photoresponsive behavior of the bR-PV cell, the device was initially exposed to a series of three consecutive light pulses by using a mechanical shutter with varying time durations, as shown in Fig. 11. Under dark conditions with no external illumination, the bR thin film exhibits a measurable voltage difference across the electrodes in the range of 0.6 to 0.8 mV. The small voltage recorded in the dark state confirms the existence of a difference in charge density between the cytoplasmic and extracellular sides of the bR PMs.[32,62,65]

The influence of light intensity on the photocell's response was also investigated by varying the light power of the source from 0% to 100%, as shown in Fig. 12.[33] Previously published research[66] showed that there is a near-linear relationship between input light intensity and the photovoltage response of a bR film. However, these results were observed for a thicker (~30 μm) dried bR film fabricated using the EFS immobilization method. The nonlinearity observed in the current study may reflect the differences in charge density of the highly oriented PMs embedded in the ultrathin monolayer and the less uniformly oriented, and stacked, PMs in the thicker EFS-formed layer.

4.2 Aqueous bacteriorhodopsin photovoltaic cells

When exposed to light, the aqueous bR-PV cell (Fig. 13) acts as an electrochemical device that pumps H^+ ions across a porous membrane creating a measurable potential difference. Al-Aribe et al.[10] demonstrated that an ultrathin layer (~13 nm) of oriented PM patches can be self-assembled on an Au-coated porous anodic alumina substrate using the biotin labeling and streptavidin molecular recognition technique described in Section 3.2. The average pore diameter of the

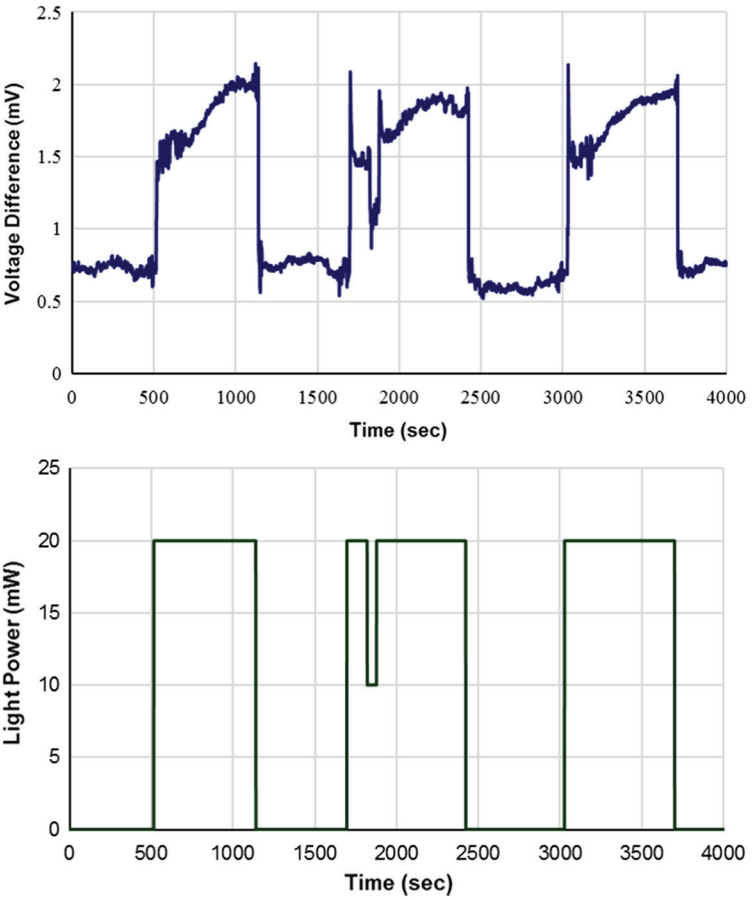

Figure 11 Measured voltage difference across the bR film on a 0.185 cm^2 substrate as a function of light exposure time. Three pulses with increased time durations of light exposure are shown (Western University).

biofunctionalized substrate is 100 nm. This porous substrate, which is coated with the labeled bR, works as a pumping station that allows only the pumped protons to pass through, whereas the same biofunctionalized substrate works as an electric barrier that does not allow the unwanted ions to migrate between the two ionic solutions. The photoinduced proton pumps generate a flow of ions that produce a measureable change in pH for the ionic solutions, in reservoirs R1 and R2, separated by the porous substrate barrier.

To measure the potential difference, platinum wire probes are inserted in the opposing liquid reservoirs near the porous bR monolayer. The platinum wire is used for electrochemical stability. Once assembled, the probes are connected to a volt meter, and the photoelectric response characteristics of the bR-PV cells are measured under fixed light wavelength and intensity conditions. The ionic

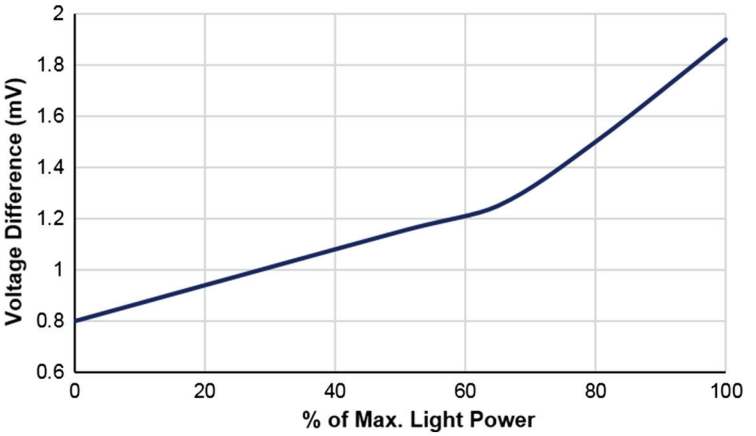

Figure 12 Relationship between light intensity and dry bR-PV photocell response.[33]

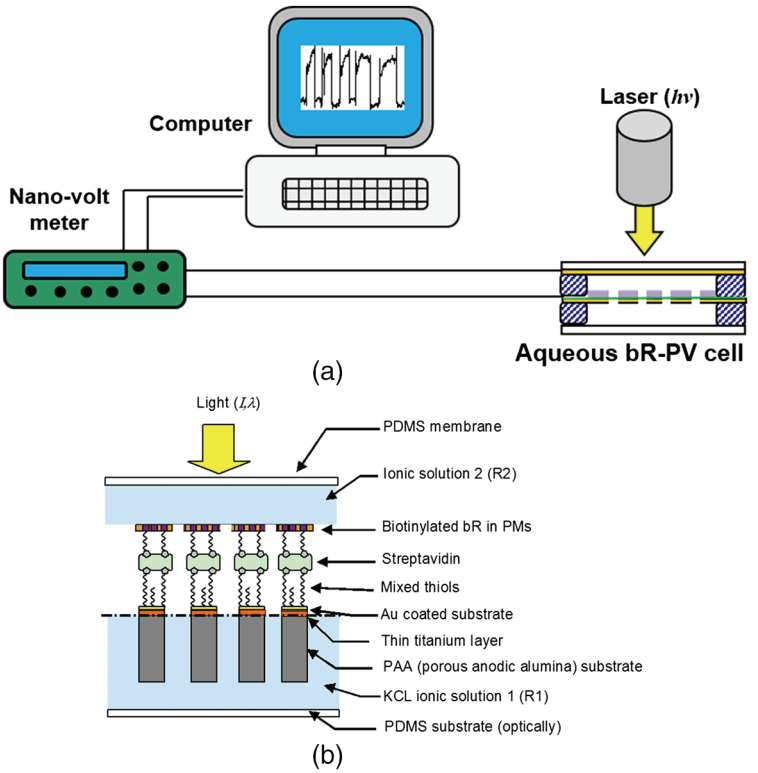

Figure 13 (a) Experimental apparatus and (b) illustration of the optically driven pH gradient generator used to transport hydrogen ions between two adjacent ionic solutions separated by a porous substrate.

solution that filled the reservoirs for these tests was 200 mM KCl. Once more an 18-mW, 568-nm light source is used in the experiments because the peak photoexcitation of bR occurs at this wavelength. The voltage differences (Fig. 14) were measured using an Agilent 34420A nano-volt/micro-ohm meter. No additional signal processing or amplification was performed in an effort to minimize distortions to the experimental readings.

When the light strikes the photoelectric part of the device, a relatively fast photovoltage of 2 mV is produced followed by a continuous increase in photovoltage up to an accumulated voltage difference of 4 mV. The electrochemical bR-PV cell was then tested under different conditions when connected to an external resistance of 1.0 kΩ to record the voltage. The photovoltage with an external resistance is smaller than the bR-PV cell's response without the external resistance. This result is expected because the overall resistance of the circuit is increased, reducing the amount of current flowing through the cell. The photocurrent is usually calculated from the measured photovoltage.[67] The recorded photocurrent shows a consistent build-up when the cell is exposed to light beams. This response reflects the optical activity of the bR proton pumps. The generated photocurrent is characterized with its negative sign, which arises from the nature of the current as it is a current of positive charges.[68,69]

One area of recent interest has been the design and nanofabrication of optically driven transducers that can change the pH of a target solution in a microfluidic channel or reservoir. To explore this in greater detail, a small set of experiments was performed by Al-Aribe et al.[10] on a 0.2-cm^2 transducer. The tests showed that the bR-PV could generate pH gradients as high as 0.42 and absolute voltage differences as high as 25 mV when illuminated by the 18-mW, 568-nm light source (Fig. 15). Further tests show that the change in pH is nonlinear with

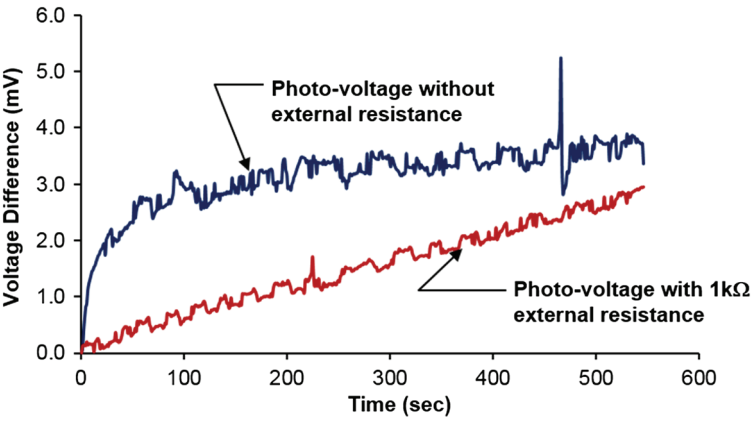

Figure 14 Measured voltage difference across the bR layer on a 0.096 cm^2 substrate under continuous light exposure. The aqueous bR-PV photovoltage measured both with and without an external resistance is shown (Western University).

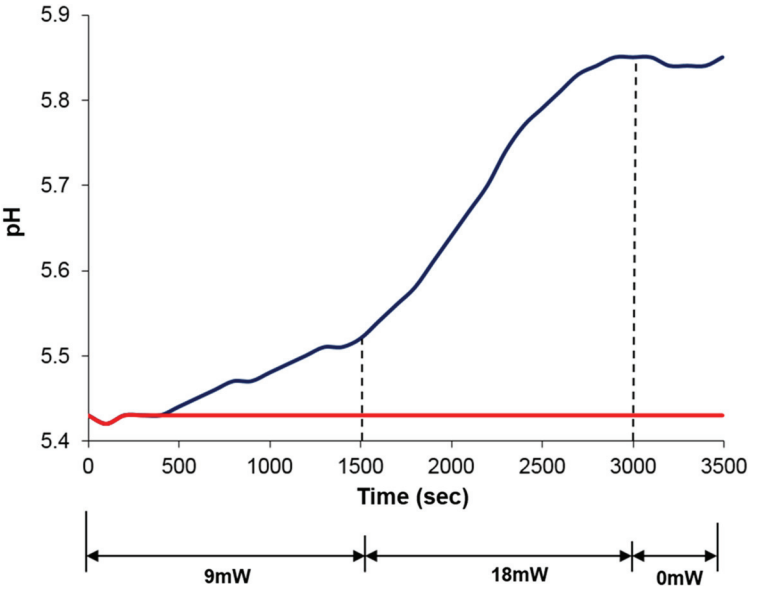

Figure 15 The change in pH of the ionic solution as a function of light exposure.[10] The pH gradient transducer has an active surface that is 0.2 cm^2.

respect to light intensity and exposure time. The rate of change is also a function of the biofunctionalized surface area and the volume of the separated ionic solutions.

5 Biological Light Switches and Photodetectors

Photoresponsive proteins that directly convert photons into a measured electrical signal have been studied extensively by a number of biochemists and biophysicists in the past half century.[70] In this regard, bR is the most notable because it exhibits light-sensitive characteristics similar to that of the rhodopsin found in the human eye. In contrast to other protein photoreceptors, bR is also highly resistant to thermal and photochemical degradation, thereby exhibiting excellent long-term stability for creating optical devices and bioelectronic photosensors, including optical memories,[2,70] optical computing,[71] optical switches,[25] photocells,[1,72,73] image processing,[74–76] motion detection,[1,77] and color vision.[78,79]

5.1 All-optical switch based on bacteriorhodopsin-coated microresonators

All-optical switches are devices that enable one light signal to control another light signal. In telecommunication systems, the optical switch is used to switch between signals in optical fibers or integrated optical circuits. Mechanical switching between fibers is very slow so alternative methods that exploit electro-optic

effects, magneto-optic effects, or new photonic materials are often considered. To achieve the desired high-speed performance of many light-wave communication systems, it has been the goal of many engineers to utilize only light. A solely photonics approach to switching requires the optical switching device to have very small physical dimensions in an effort to increase speed, improve reliability, and reduce unit cost. To achieve these goals, researchers have explored new materials with strong optical responses and developed microresonating components that can amplify the naturally weak light–material interactions.

Optical microcavities[80] and microspheres[81,82] can function as light-wave resonators for all-optical switching applications.[83] These resonators reflect the light multiple times to produce standing waves at a predefined resonance frequency. Significant work has been done in miniaturizing the optical cavities.[81] These developments have also been achieved by using optical materials that exhibit nonlinearities. The all-optical switches exploited shifts in the photochromatic material's refractive index,[84] generating anisotropy[85,86] and shifting the absorption bands.[87] However, successful implementation of photochromatic microcavities for switching in the optical fiber telecommunication wavelength (1311 to 1550 nm) requires a material with high optical responsivity.[81,82]

To physically realize a photochromatic light-driven switch, Topolancik and Vollmer[81] proposed coating a resonating silica microsphere with bR because this biological photoreceptor is able to influence the frequencies of the interacting resonance modes when triggered with optical signals. In essence, the control light signal drives the bR protein to undergo all-*trans* to 13-*cis* structural changes. The optically driven changes are used to generate an all-optical tunable resonant coupler. To demonstrate this concept,[81] three monolayers of genetically modified bR (D69N) were deposited on a 300-μm silica sphere using alternate ELBL adsorption of PDAC and the bR fragments (Fig. 16). The prototype's silica microsphere is made by melting a single-mode optical fiber using a butane-nitrous oxide flame.[81] Genetically modified bR (D69N) was used to ensure a prolonged *M* state for reliable and complete conversion between the all-*trans* and 13-*cis* states.

Once deposited on the silica microspheres, the bR showed the ability to reroute the low-power laser beam between two optical fibers, as shown in Fig. 16(b). The resonant coupler was operated at near-infrared wavelength (1311 nm) while the green light excitation pump (532 nm) was operated at less than 200 μW. The bR-coated microsphere was inserted into a 1-cm acid-resistive, polystyrene-based cuvette. The cuvette is shaped by using hydrofluoric acid to be able to insert two parallel single-model fibers separated by a distance of 250 μm. Before inserting the silica microsphere, the optical fibers were immersed in a phosphate buffer with an ionic strength of 0.01 M and pH of 7.4.

After the optical fibers became stable, the bR-coated silica microsphere was loaded between the fibers. The positioning of the bR-coated microsphere between the two optical fibers forms a four-port tunable resonant coupler. The optical

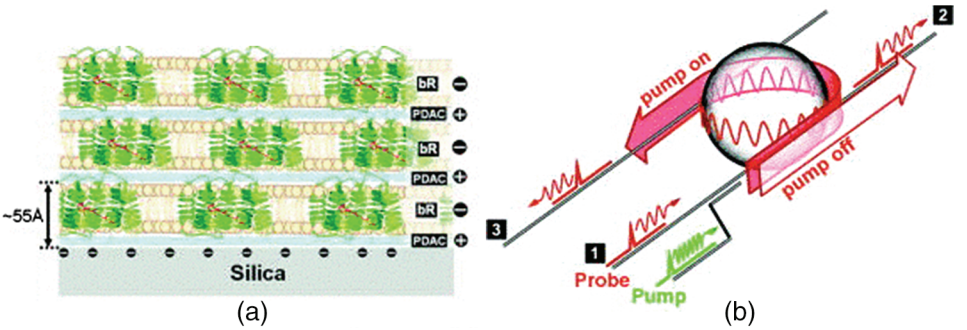

Figure 16 (a) Fabrication and (b) basic function of the PDAC–bR-coated silica microsphere for all-optical switching. (Reprinted from Ref. 81, with the permission of AIP Publishing.)

switching of the near-IR source (port 1) between the two output ports (2 and 3) is driven by a green laser that controls the conformational state of the bR immobilized on the microsphere. In other words, the biomolecularly functionalized microsphere redirects the flow of the near-IR light between port 2 and port 3 based on the state of the bR. A near-IR laser (1311 nm) was connected to port 1 to excite the resonant modes and the modulation current was scanned at 100 Hz to find the resonance wavelength. Photodetectors were connected to fiber ports 2 and 3 to measure light intensity and wavelength. The sampling time for the output signal was 200 ms.

Figure 17(a) shows the bR-coated microsphere positioned between the two experimental fibers when both all-*trans* (green light pump off) and 13-*cis* (green light pump on) states exist. It is clear from the figure that the input near-IR light can be directed either toward port 2 (C) or port 3 (D). Figure 17(b) represents the measured resonant transmission spectra when the bR is in the all-*trans* (port 2) and 13-*cis* (port 3) states. Note that with the green light pump off port 2 shows a high transmission, and port 3 shows a low transmission at 1311.039 nm. This is shown by the dark curves in Fig. 17(b). Conversely, when the pump is on, the reverse is observed, as shown by the gray curves in Fig. 17(b).

In terms of all-optical switching, the dynamics are determined by the speed of the bR photochromatic transitions.[81,83] Additional research had shown that a fast transient time is associated with the phototransformation from the ground state to the *M* state and a slower time is associated with the thermal ground state recovery. These observations indicate that although bR-coated microresonators are effective and perform as expected, there is a need to improve the biomaterial response to increase the overall switching speed.

5.2 Bioelectronic photodetectors and imaging arrays

bR's thermal stability and high quantum efficiency, coupled with well-understood photochromic and photoelectronic properties, make it a promising biomaterial for

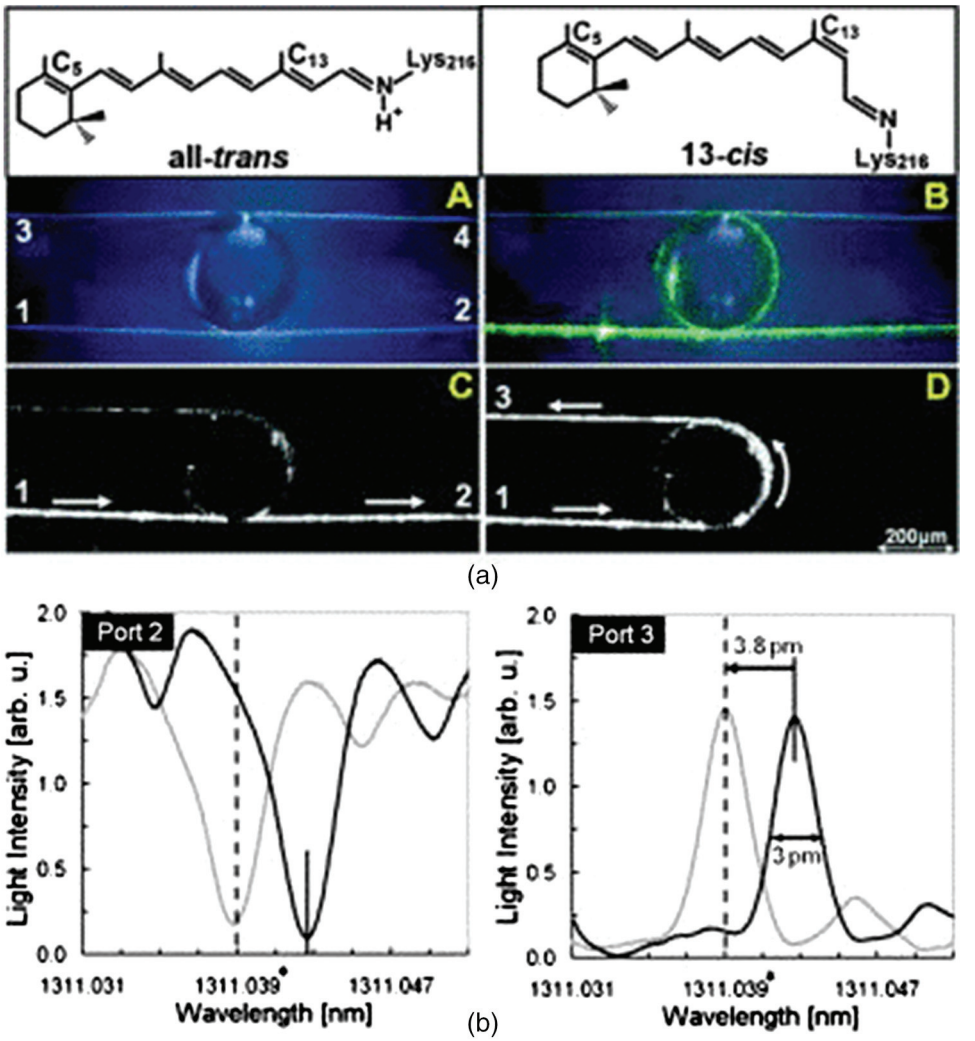

Figure 17 Photographs of the bR-coated coated microsphere positioned between two fibers under different states of illumination and the measured resonant transmission spectra when green light pump off (all-*trans*) and pump on (13-*cis*). (Reprinted from Ref. 81, with the permission of AIP Publishing.)

developing light-sensitive biosensors and photodetectors.[19,72,78] However, proper immobilization of bR molecules to charge-sensitive substrates is required to utilize such photosensitive properties. Widely adopted substrates include silica glass coated by conductive oxides, such as tin oxide or ITO, and metal electrodes, such as gold and platinum.[88] Some new substrates have emerged enabling micro/nano applications. These include the gate terminal of a GaAs-based MOSFET and nano-black lipid membranes.[40,50]

A number of membrane-based bioelectronic devices have been reported in the literature. One example is an 8×8 pixel array of bR photocells fabricated by Miyasaka et al.[57] for the purpose of image detection. The bR film is uniformly deposited on an ITO pattern on a glass substrate using the LB method. The resultant bR film is then covered with an aqueous electrolytic polymeric gel layer and a gold electrode to complete the sandwich-type structure. Haronian and Lewis[89] investigated methods that allow microfabrication of bR without losing its photoelectronic properties. A bR array with 50 μm × 50 μm pixels is created by depositing bR onto an ITO electrode and then ablating both the film and substrate using an argon fluoride excimer laser. A novel protein-silicon hybrid photodetector array was proposed by Birge and his group.[90,91] To construct the high-resolution bR-silicon photosensor, the detection grid of a charge injection device (CID) is utilized as the substrate for a thin bR-polymer film. This architecture also incorporated processing circuitry to monitor the photoresponse of the bR film. Researchers in Italy demonstrated a compact bR microarray, which is fabricated by patterning dehydrated bR films on microstructured Si and SiO_2 surfaces without orientation.[92]

Many of the bioelectronic photodetectors and multipixel imaging arrays are fabricated on rigid substrates using conventional electrodes and printed circuits.[78] For example, a multipixel grayscale imaging array can be created by immobilizing continuous bR films on a 2-D array of square electrodes on the printed circuit board. Lensu et al.[78] created such a device by first immobilizing wild-type bR PM fragments in a PVA gel and then spreading it on the individual pixels of the array. A thin layer of Au was then sputtered on top of the bR-PVA film to form a counter electrode. The wild-type bR-PVA elements in the imaging array had an average thickness of 144 μm with a standard deviation of 26 μm. Experiments showed that this simple design provided high quantum yield and repeatability. The wavelength of maximum absorbance for the wild-type bR is 412 nm at the dark-adapted state and 568 nm at the light-adapted state (close to the *L*-cones in the human retina). Furthermore, the photoelectric response was linearly dependent upon the number of bR molecules per unit distance in the direction perpendicular to the electrodes. This implies that the film thickness and variations in the film thickness for the different elements will affect the quality of the results.

The ability to build photoelectric monolayers and thin films on a variety of non-rigid substrates offers design opportunities not possible with traditional rigid silicon-based microelectronics (e.g., CMOS). In terms of design, the single and multispectral bioelectronic sensing technology fabricated on bendable plastic substrates can lead to significant reductions in spatial requirements, weight, electrical power consumption, thermal heat loss, system complexity, and fabrication cost. For example, the direct deposit of photoelectric materials onto low-cost flexible ITO electrodes enables design engineers to create innovative lightweight, durable, and nonplanar sensing surfaces. By fabricating patterned arrays on bendable plastic substrates, it is possible to develop photoresponsive sensors that can be either

rolled up when not in operation or permanently adhered to nonplanar surfaces. Unlike traditional flat, rigid silicon-based CMOS and CCD image arrays, bR-PET-ITO imaging systems with curved geometries can provide information processing advantages, such as an increased field of view or enhanced focusing capabilities.

A bendable 175-μm-thick polyethylene terephthalate (PET) film has been used by Wang[64] and Wang et al.[1,18,19,31,59] as the substrate material for creating patterned sensor arrays. PET is a common plastic that is inexpensive to manufacture, has mechanical durability, and exhibits high light-transmission properties (typically >86%). A conductive ITO layer is deposited onto the flexible substrate via pulsed laser deposition (Sheldahl Inc.). The ITO-coated film has a surface resistance of 35 Ω/sq. The electrode is imprinted with a 4×4 pixel pattern (Fig. 18), where each pixel is 2 mm $\times$ 2 mm and is separated by 1 mm between neighboring pixels. Independent ITO wires, each 300 μm wide, connect the pixel with a connection terminal along the substrate edge. The overall area of a patterned ITO electrode is 15 mm $\times$ 23 mm.

The fabrication conditions, such as the electric field intensity, exposure time, and ambient drying humidity, were all found to affect the photoelectric response and topology of the dried bR film. Experimental tests showed the noticeable aggregation of bR PMs that lead to decreasing the photoelectric responsivity. Excessively high electric field intensities not only reduce aggregation but also reduce photocell performance due to protein degradation.[74] An intermediate electric field (~40 V/cm for 5 min) produced good results.[59,64] Relative humidity in the range of 50% to 60% typically yielded bR films that produced the highest photocurrents.[93]

Engineered photodetectors are often characterized by their linearity over a given dynamic range and spectrum. A photoreceptor is considered linear if the

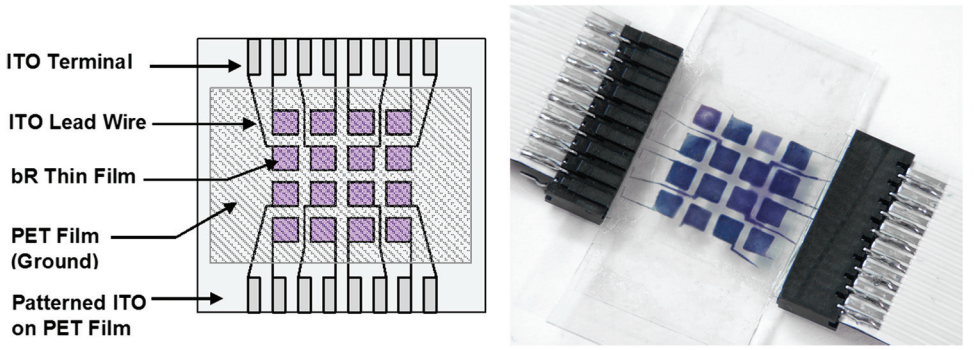

Figure 18 (a) Schematic diagram and (b) photograph of an experimental 4×4-pixel bR-ITO-PET photoreceptor array constructed from two mechanically flexible ITO-PET layers (Western University).

generated photocurrent increases proportionally in a linear relationship to the incident light power or intensity. The maximum signal level detected by a bR-based photoreceptor is recorded at its saturation level, and the lowest level of the detectable light is limited by system noise. The peak differential response of a bR photoreceptor is noted to vary linearly with changes in light intensity between the upper and lower limits. The bR material exhibited high sensitivity as it responded to very small changes in the input light intensity. This property was investigated experimentally using a tunable argon/krypton laser system with nine selectable wavelengths ranging from 476 nm (blue) to 676 nm (red) (Melles Griot, 35KAP431-220). The linearity of a single bR photoreceptor pixel was tested for three wavelengths (488, 568, and 647 nm; Fig. 19), where the beam intensity is adjusted over the light power range between 200 μW and 10 mW.[64]

Multiple bR elements can be used to create a motion-detection sensing array that identifies both the direction and speed of movement.[64] The Reichardt model of movement detection[94] employs temporal edges as the image features and correlates them by using binary pulses,[19,31,59] as shown in Fig. 20.

The motion-detection architecture has three basic parts: feature extraction, pulse generation, and speed detection. First, the photocells PR_1 and PR_2 transform the incident light into electric signals, and edge-detector circuits are used to generate a current pulse that corresponds to temporal edge information. Second, the resultant current pulses are transformed into voltage pulses by a separate pulse generator circuit. This pulse generator includes a pulse-holding circuit that adds a delay to the voltage pulse. Third, the transient pulse is then correlated with the delayed pulse, and a positive (or negative) output pulse is produced only when the object moves in the desired direction. Note that the overlap width of the two pulses from the previous pulse holding stage contains the velocity information.

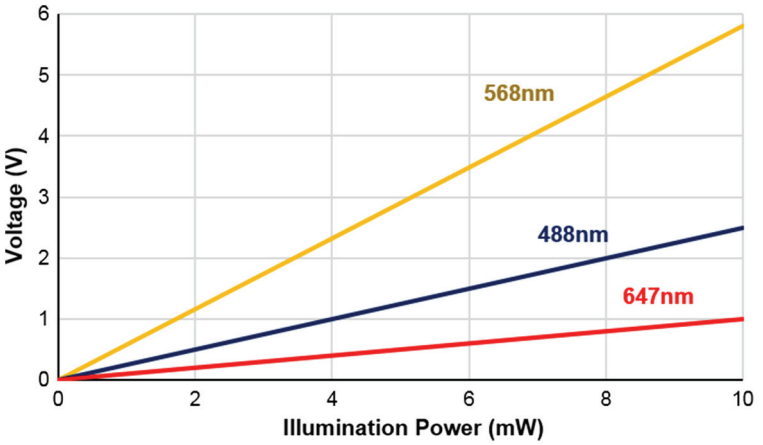

Figure 19 Observed linear response of a bR photoreceptor over varying wavelengths (488, 568, and 647 nm) and illumination power (Western University).

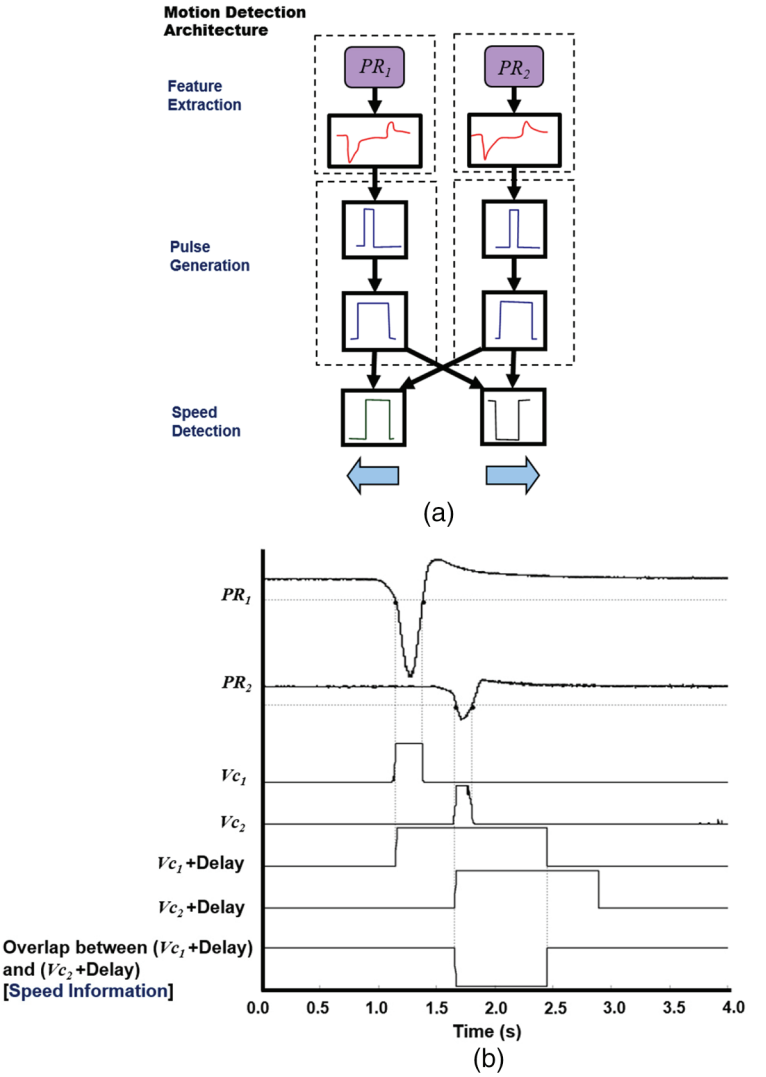

Figure 20 (a) Block diagram of the modified Reichardt's correlation model used for motion detection by the 4×4 bR-ITO-PET array (Fig. 18).[64] (b) Examples of recorded waveforms for the different motion detection stages as a light spot moves from left to right at a speed of 40 mm/s. Note that PR_1 and PR_2 are the photocells, V_{c1} and V_{c2} are the output signals generated by the voltage comparators, and (V_{c1} + delay) and (V_{c2} + delay) represent the sample delay that is applied to the input signals. The overlap between the two delayed pulses contains the speed information.

Finally, motion is determined by correlating the delayed digital input from one pixel with the appearance of a digital signal from a neighboring pixel.

The prototype array was experimentally tested by detecting a moving light spot generated by a 2-D laser scanning system. A tunable argon/krypton laser

system was used as the light source, and a two-axis acousto-optic deflector (AA.DTS.XY-250) scanned the laser beam across the array surface in a single direction. A two-channel function generator was applied to control the beam deflection angle in each direction. The bR-based motion detector simplified the system circuitry by exploiting the temporal filtering behavior of the dry bR film. Real-time motion estimation was achieved for velocities ranging from 20 to 80 mm/s.[59]

5.3 Color-sensitive imaging using bacteriorhodopsin photodetectors

Color imaging can also be accomplished by utilizing a spatial array of photodetectors, where three types of sensing elements with different spectral sensitivity properties (e.g., red, green, blue) are used. For high accuracy and informationally complete applications, the imaging sensor may actually have more than three sensing components. Furthermore, the sensing elements must be designed to capture the desired information from the energy spectrum and provide a high signal-to-noise ratio (SNR) for good color discrimination. To investigate the viability of using bR for color imaging, Lensu et al.[78] developed a bR color-sensitive biosensor array. The authors used retinal substitution to modify the spectral properties of the bR and create three sensing elements that correspond to the wild type of bR; wild type of bR reconstituted with 3,4-dehydro; and wild type of bR reconstituted with 4-keto.

The individual elements of the color-sensitive bR imaging array are coated with one of the three types of bR. The selected bR material was mixed with a polyvinylalcohol (PVA) and phosphate buffer solution, and then deposited on the individual conductive elements (i.e., pixels) of the printed circuit board. In this manner, the bR was immobilized by the gelation of the PVA. A thin layer of Au was sputtered on top of the bR-PVA film to create the counter electrode for the sandwich structure. The film thickness of the individual elements was roughly 101 to 107 μm with a standard deviation of 16 to 20 μm.[78] The typical layout of the different array elements is shown in Fig. 21. The three types of bR are wild type, 4-keto, and 3,4-didehydro. The electronics in this experiment included an instrumentation amplifier, signal amplifier, peak-hold circuit, and buffer circuit. A microcontroller was used to digitize and process the peak photovoltages produced by each element in the array.

The photoelectric response and action spectra of the elements in the imaging array were measured and the sensitivities calculated[78,79] to evaluate sensor performance. The normalized photoelectric response and element absorbance for various wavelengths (400 to 700 nm) is shown in Fig. 22. However, the investigation by Lensu et al.[78] determined that the dynamic range and the number of detectable intensity levels were a function of the number of bR molecules in the sensor element, SNR of the electronics, resolution of the analog-to-digital conversion, and the shutter mechanism.

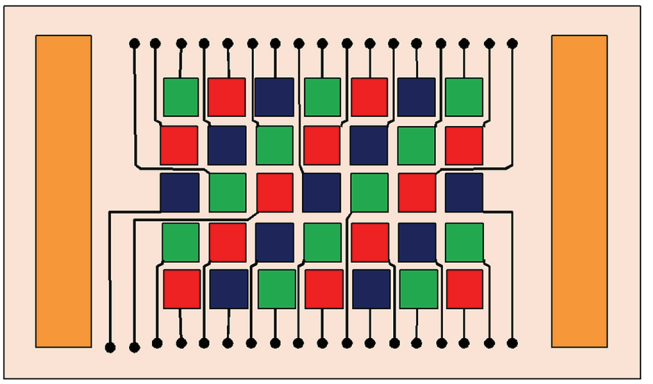

Figure 21 The layout of wild-type (red), 4-keto (blue), and 3,4-didehydro (green) films on the printed circuit board. (Adapted from Ref. 78.)

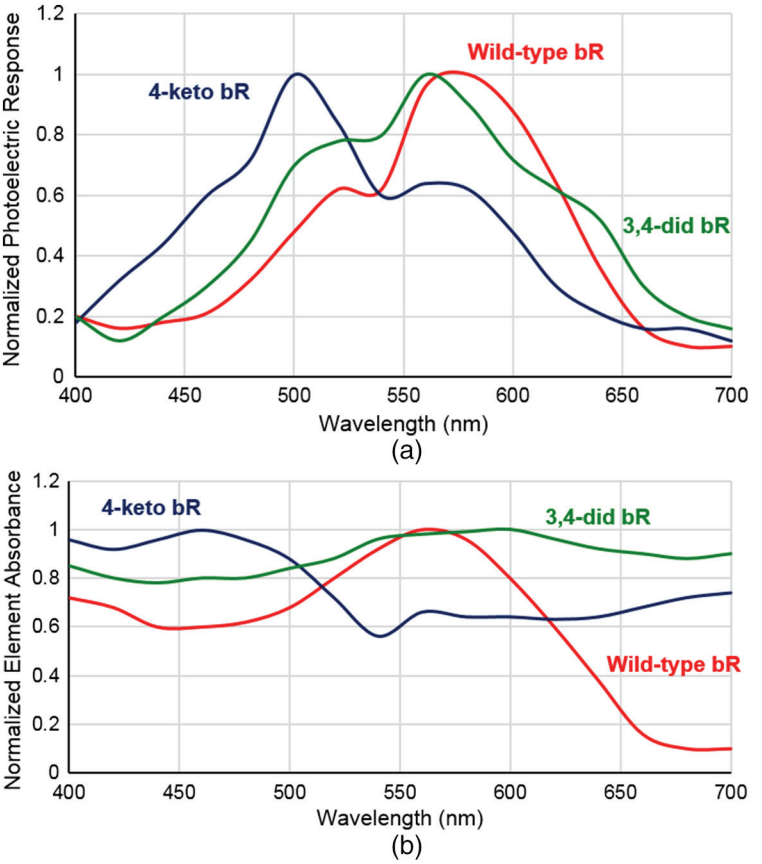

Figure 22 (a) Normalized photoelectric response and (b) element absorbance spectra for wild-type (red), 4-keto (blue), and 3,4-didehydro (green) films. (Adapted from Ref. 60.)

To demonstrate the capability of the color-sensitive imaging system, a couple of test images based on the GretagMacBeth™ color rendition chart and spectral image of a natural scene were examined. The pixel resolutions of the test images were 64×64 and 256×256, and the number of spectral bands was 151 and 31 (400 to 700 nm at 2 nm and 10 nm intervals), respectively. The response images showed that the imprecision in the measured action spectra caused limited color-discrimination capability.

The spectrum of the three types of bR photosensors does not directly correspond to the color *L*-, *M*-, and *S*-cones in the human retina. These biological photoreceptors are maximally sensitive to long wavelengths (*L*-cone), sensitive to medium wavelengths (*M*-cone), and sensitive to short wavelengths (*S*-cone). To relate the bR responses to perceived color, Lensu et al.[78,79] developed a mapping function using a neural network called a self-organizing map (SOM). The SOM is often used to correlate topological associations of the detected input space within its predefined lattice.[95] In essence, the continuous space of color signal patterns (inputs) is mapped into a discrete network or lattice of nodes (outputs) using an unsupervised adaption process.[96] Once trained, the SOM can be used to locate an appropriate node within the predefined lattice. When the templates developed for visual pigments were fitted to the absorption peaks of the three bR types, the results showed a closer correspondence to the *L*-, *M*-, and *S*-cone pigments of the human retina.[78]

6 Light-Driven Ionic Polymer Microactuators

Monitoring and regulating the pH of solutions is an important step in controlling a variety of biological and chemical processes on lab-on-a-chip (LOC) devices and micrototal analysis systems. Externally modifying the pH of a target solution can drive a variety of electrochemical processes necessary to identify unique proteins, move molecules,[97] and exchange ions between solutions.[98] Other LOC applications that depend on the generated pH gradients are the fractionation, separation, and assembly of biologically based molecules, such as the human salivary proteins and the collagen bundles.[99] Manipulating the pH of a solution in a microchannel, or reservoir, also provides a mechanism for activating and controlling an ionic hydrogel microactuator, or the color of a phenolphthalein indicator dye for visually monitoring the acidity changes in sample solutions.[100]

Microactuators are often very small material structures and mechanisms that perform mechanical work in response to external stimuli. The resulting mechanical action is able to generate tiny displacements or induce microforces on the surrounding medium. The expansion and contraction of the hydrogel under environmental stimuli has been used to regulate the flow of liquids in a variety of microfluidic systems.[101–104] The advantages of hydrogel over other deformable

microactuator shells are its relatively simple fabrication, no external power requirements, no integrated electronics, significant displacements (up to 185 μm), and relatively large force generation (~22 mN).[10,100]

Hydrogels undergo large conformational changes, causing swelling/deswelling when exposed to a variety of environmental stimuli including changes in pH, temperature, and light. The pH-sensitive hydrogel containing hydroxyethyl methacrylate-acrylic acid (HEMA-AA) has been extensively used for microvalves and micropumps in fluidic systems. This environmentally sensitive hydrogel undergoes abrupt volumetric changes when the pH of the surrounding medium increases slightly above the phase transition point pKa. If the networked gel is immersed in an ionic aqueous solution, then the polymer chains will absorb water, and the association, dissociation, and binding of various ions to the chains will cause the hydrogel material to swell, producing a usable microforce.

Although the absence of any external power source has been promoted as an advantage of a smart gel, the response times of direct chemical to energy conversion are often impractical requiring several hours for the gel to fully respond to changes in solution pH. Furthermore, using the pH as a control mechanism limits the number of components that can be independently controlled and requires all the components to be compatible with the requisite changes in pH.[105] The downside is that many microfluidic applications are not compatible with a large range of pH values. In other applications, it is beneficial to have independent external control.

6.1 Optically driven pH gradient transducer

A low-power optically driven pH gradient generator provides an alternative noninvasive mechanism for modifying the target solution's acidity without inducing strong electric fields near the solution or exposing the working solution to high-intensity illumination and heat. Eroglu et al.[106] described a simple biologically inspired pH gradient generator based on the light-harvesting bR protein. The authors also concluded that proper directional orientation of bR PMs is a critical factor for efficiently pumping H^+ ions in microfluidic channels. Based on this early work, Al-Aribe et al.[10] developed a more efficient pH gradient transducer from self-assembled bR PMs on a rigid nanoporous anodic alumina (PAA) membrane (Fig. 23).

The molecule self-assembly technique described in Section 3.2 was used to create an ultrathin functional layer where all bR PMs were aligned in a consistent orientation. The PAA membrane provided a separation barrier between the ionic solution that surrounds the gel microactuator and the KCL buffer solution. The active surface of the bR-PAA transducer is 0.2 cm. The actuator shell is a cylindrical HEMA-AA gel plug constructed in a microfluidic channel. The principle of operation is that when the transducer is exposed to visible light (568 nm), the

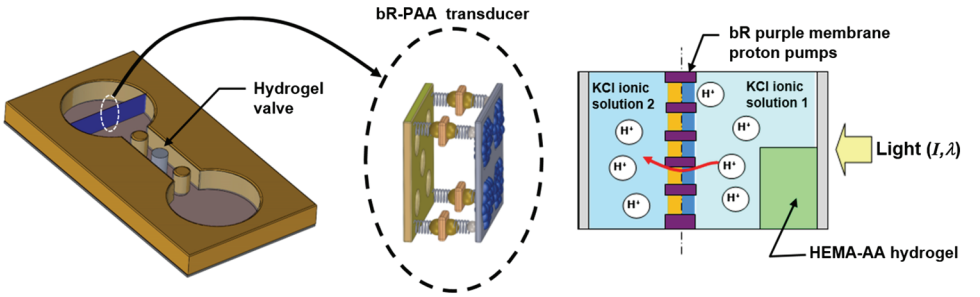

Figure 23 Illustration showing the insertion of the light-activated nanoporous bR-PAA transducer in a microfluidic chip reservoir and the basic mechanism for transporting H^+ ions between the two separated KCL ionic solutions.[10]

protons (H^+) in the solution around the actuator flow to the KCL buffer solution, causing swelling action of the HEMA-AA microactuator.

The light source for the experimental tests was an 18-mW Melles Griot Argon Ion laser (568 nm, 18 mW) with a mechanical shutter and optical fiber angled at ~60 deg with the horizontal to deliver uniform illumination across the entire photosensitive surface of the bR-PAA transducer. Under dark conditions, the bR-PAA transducer showed no measurable changes. However, when the monochromatic light first illuminates the active transducer surface, the bR PM proton pumps start to transport H^+ ions from the ionic solution at the transducer's interface to the ionic fluid in the opposite reservoir through the nanoporous membrane. The change in H^+ ion concentration in the solutions of reservoir 1 (R1) and reservoir 2 (R2) is shown in Fig. 24.

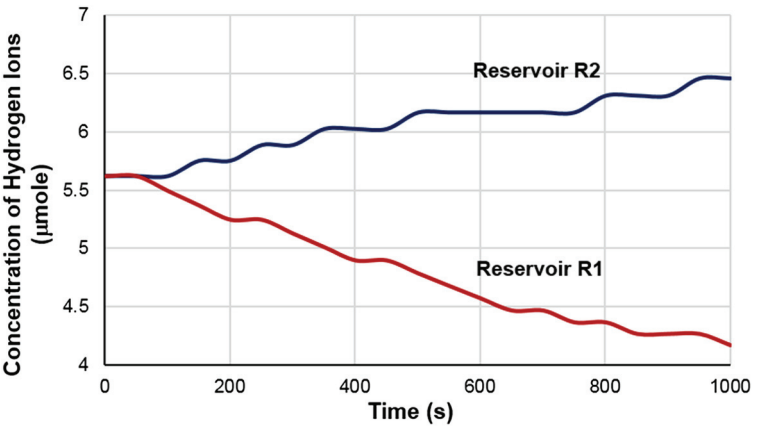

Figure 24 Change in H^+ ion concentration over time of the two reservoirs separated by the bR-PAA transducer when exposed to an argon ion laser (568 nm, 18 mW).

The change in H^+ ion concentration is also a function of the light intensity, as shown in Fig. 25. Note that the dashed line at an H^+ concentration of 3.7 μmol shows no change in ion concentration when the bR-PAA transducer is in a dark state (i.e., 0 mW) for 3500 s. The curve shows the concentration of H^+ ions when the transducer is exposed to 5 mW for 1500 s and then 18 mW for another 2000 s. Note that around 3000 s, the concentration of H^+ ions reached a steady-state value around 1.5 μmol due to the depletion of the hydrogen ions in the working solution. In general, the ion concentration is decreased, producing an increase in the solution's alkalinity. Simultaneously, these mechanisms increase the concentration of the hydrogen ions, and thus increase the acidity of the liquid in the opposite reservoir (R2).

The measured pH changes in the solution are also a function of the light intensity. These results indicate that a minimum level of light energy is necessary to activate the bR proton pumps and alter the solution's pH. Note that the nonlinear behavior is not unexpected as the observed pH change is the combined activity of the bR's proton pumping action (which is inherently nonlinear) and the electrostatic interaction of ions transported across the bR-PAA transducer. The light-driven bR proton pumping action instantaneously depletes the concentration of the hydrogen ions at the interface of the bR surface with the ionic fluid. This depletion is compensated by diffusion of hydrogen ions from higher-ion-concentration regions in the same reservoir. However, the electrostatic repulsive forces between the mobile ions will randomly displace in the solution until the concentration is homogenized.[50]

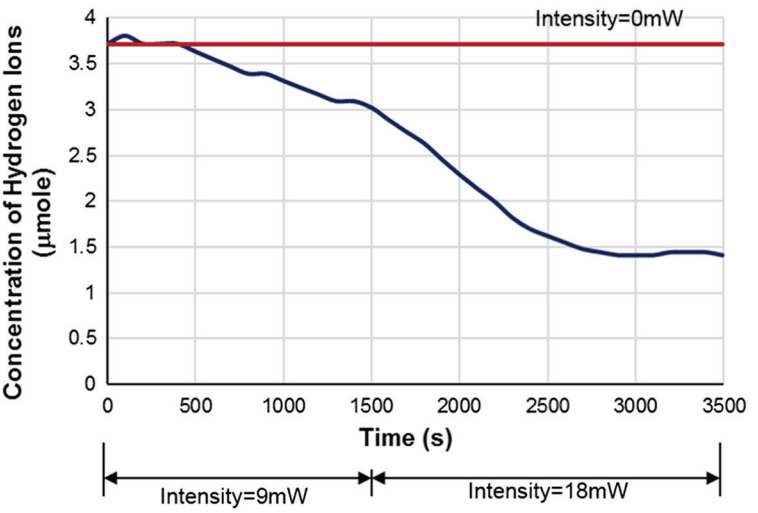

Figure 25 Change in H^+ ion concentration of the solution in reservoir 1 as a function of exposure to different levels of light intensity (0, 9, and 18 mW).

6.2 Hydrogel microactuator activated by bacteriorhodopsin proton pumps

The primary mechanism for generating a displacement, force, or pressure is the expansion and contraction of the hydrogel actuator shell in response to a ΔpH of the surrounding solution. To externally control the volumetric transformation, a light-responsive proton pump is used to generate a unidirectional flow of ions through the nanoporous membrane that increases or decreases the pH of the two separated ionic solutions. The pH gradient creates an ion concentration difference between the inside and outside of the gel structure causing some H^+ ions to move across the gel and thereby producing an osmotic pressure difference across the gel structure. If the osmotic pressure generated by ion movement into the gel exceeds the outside pressure, the internal forces will cause the tangled networks of cross-linked polymer chains to expand outward, and the hydrogel will swell. If the networked hydrogel is immersed in a suitable ionic solution, then the polymer chains will absorb water and the association, dissociation, and binding of various ions to these chains will cause the hydrogel material to enlarge, producing a usable microforce.

Two important design considerations for developing a pH-sensitive microactuator are the size of the hydrogel actuating shell and the ion concentration of the solution that surrounds the gel. The primary mechanism that influences the swelling response time of the gel structure is the diffusion of ions into the surrounding medium. In general, a relatively small hydrogel structure will react quicker to the ΔpH than a much larger mechanism[104,107,108] because the ion diffusion time in the gel network is dependent on the square of the diffusion length.[109] Consequently, a fabricated hydrogel structure with a large surface-to-volume ratio will have more surface exposure to the activating solution and respond faster to ΔpH. The response time of the gels can be further increased by immersing the material in a buffered solution with a high concentration of H^+ ions.[110]

6.3 Microactuator swelling analysis

The microactuator performance was evaluated by observing the geometrical changes to the HEMA-AA hydrogel actuator when the bR-PAA transducer was exposed to the monochromic light. The microfluidic device for testing and demonstrating the functional performance of the proposed pH gradient generator was a 3500-μm-diameter hemispherical chamber divided into two liquid reservoirs (R1 and R2) by a biofunctionalized bR-PAA planar transducer. Each reservoir had a maximum depth of 1750 μm from the chip's surface and held ∼100 μL of 100 mM KCL ionic solution. The R1 reservoir had an output channel with a width of 150 μm and a depth of 100 μm. The hydrogel actuator (Fig. 26) had a diameter of 75 μm and a length of 100 μm. The chip was filled with an ionic

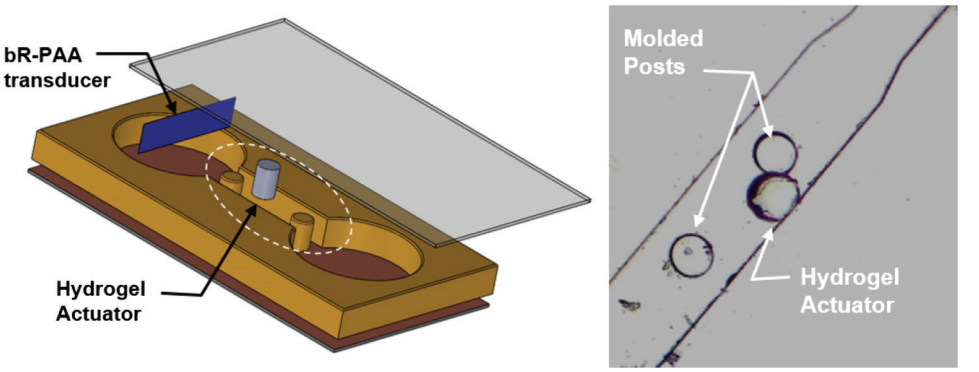

Figure 26 Schematic and photograph of the HEMA-AA gel actuator in the microchannel with an ionic solution that has a pH equivalent to reservoir R1.

solution of KCl with an ionic strength of 200 mM and at a pH of 4.4. The pKa of the acrylic acid-based hydrogel was 4.7.[111]

For this investigative study, the pH-sensitive hydrogel was allowed to expand freely in the microchannel without any structural constraints. To prevent evaporation and contamination, the experimental PDMS microfluidic chip was covered by 100-µm-thick glass and sealed with an adhesive. The light source (18 mW, 568 nm) was delivered to the active photoresponsive side of the bR-PAA transducer using a flexible optical fiber. Physical changes to the volume, length, and diameter of the hydrogel were observed within the first 5 min. The recorded measurements showed a volumetric change of more than 80% in less than 85 min. Similarly, increases in length and diameter of 22% and 23%, respectively, were observed.

The pH-sensitive HEMA-AA hydrogel actuator was also examined for the swelling reversibility (Fig. 27). The direction of the ion flow into the working

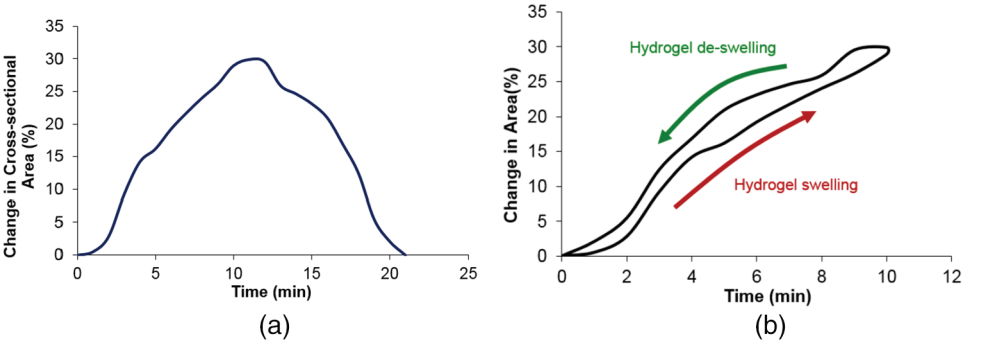

Figure 27 Changes in (a) cross-sectional area and (b) the observed hysteresis effect when H^+ ions flow out of and then into the working solution (Western University).

solution was reversed by introducing a second bR-PAA transducer that acted as a second independent proton pumping station. The first bR-PAA transducer pumped H^+ ions into the microchannel when activated by light, whereas the second bR-PAA pumped ions out of the same channel when triggered by the light signal. Note that both were not activated simultaneously. In this manner, the expansion and contraction strokes of the microactuator material could be reversed by simply switching the light signal between these two opposite acting transducers.

The cross-sectional area had increased by 30% in the first 10 min of light exposure to the first bR-PAA transducer. At this time, the light was redirected to the active surface of the second bR-PAA transducer to increase the concentration of H^+ ions in the working solution. Once the switch in lighting direction occurred, the hydrogel would continue to expand for another minute and then remain constant for another minute before beginning to deswell. The observed time response characteristics of the swelling/deswelling HEMA-AA hydrogel were comparable to prior published results.[104,112] This observation also implied that the ion transport processes into the polymer gel network are not instantaneous producing a hysteresis effect. The nonlinear behavior is not unexpected because the driving forces behind the hydrogel swelling stroke are the osmotic pressure and the repulsive forces between the charged polymer network responsive pendant groups, whereas the shrinking stroke is dependent mainly on the fluid flow out of the polymer network. Richter et al.[111] also observed a similar hysteresis phenomenon in pH-responsive hydrogels.

7 Summary and Future Perspectives

In the 21st century, bioelectronics has emerged as one of the most influential technologies with the potential to impact a variety of areas, including medicine, personalized health care, wearable devices, public safety, and food security. As more conventional silicon-based electronics matures, its limitations in scalability and performance become more apparent. Future advances will likely require electronic components and sophisticated integrated systems that are more organic and exploit biological materials for enhanced functionality. Biomaterials are a promising alternative to traditional microelectronics because they are often physically robust, offer chemical and thermal stability, demonstrate high energy efficiency, and can be fabricated on a variety of substrates using inexpensive deposition methods.

Photosensitive proteins are one class of biomaterials that has been extensively investigated by scientists and engineers for developing enhanced sensors and optoelectronic devices. Their optical and photoelectric features permit them to behave as "smart materials" for creating innovative photocells, photoelectric biotransducers, and light-driven proton pumps. Among the various light-responsive proteins is bR, which exhibits light-sensitive characteristics similar to that of rhodopsin, a protein found in the human eye. bR is found naturally in the cellular membranes of the

salt marsh archaebacteria *H. salinarium*. When exposed to visible light, each bR molecule acts as a simple proton pump that moves hydrogen ions across the cellular PM through tiny transmembrane channels.

In terms of engineering applications, the proton transfer mechanisms of bR PMs have been used to develop a number of different optoelectronic devices, such as all-optical switching in the near-infrared spectrum, bioelectronic photodetector arrays that respond to light intensity and spectral sensitivity (i.e., color attributes), and photoelectric biotransducers for activating ionic gel actuators in microfluidic chips. Prior studies have shown that an ~13-nm thick self-assembled dry bR monolayer can generate ~10 mV/cm^2, whereas wet bR produces nearly 42 mV/cm^2. These bR films can be used to create small energy harvesting photoelectrochemical cells for powering various MEMS and microfluidic devices.

Future developments are expected to focus on optimizing the fabrication processes in order to generate zero-gap monomolecular films that are similar to the continuous membranes found in biological organisms. This will greatly improve the optoelectronic performance so that the artificial systems can approach the efficiencies observed in the original cellular micro-organisms.

References

1. W. W. Wang, G. K. Knopf, and A. Bassi, "Photoelectric properties of a detector based on dried bacteriorhodopsin film," *Biosens. Bioelectron.* **21**, 1309–1319 (2006).
2. N. Hampp, "Bacteriorhodopsin as a photochromic retinal protein for optical memories," *Chem. Rev.* **100**, 1755–1776 (2000).
3. N. Vsevolodov, *Biomolecular Electronics: An Introduction via Photosensitive Proteins*, Birkhauser Publishing, Herndon, Virginia (1998).
4. D. Voet, J. G. Voet, and C. W. Pratt, *Fundamentals of Biochemistry Life at the Molecular Level*, John Wiley & Sons, Inc., Hoboken, New Jersey (2006).
5. G. H. Krause and E. Weis, "Chlorophyll fluorescence: the basics," *Ann. Rev. Plant Physiol. Plant Mol. Biol.* **42**, 313–349 (1991).
6. D. Oesterhelt and W. Stoeckenius, "Rhodopsin-like protein from the purple membrane of Halobacterium halobium," *Nat. New Biol.* **233**, 149–152 (1971).
7. G. Váró and J. K. Lanyi, "Thermodynamics and energy coupling in the bacteriorhodopsin photocycle," *Biochemistry* **30**, 5016–5022 (1991).
8. W. Kühlbrandt, "Bacteriorhodopsin—the movie," *Nature* **406**, 569–570 (2000).
9. R. Henderson and P. N. T. Unwin, "Three-dimensional model of purple membrane obtained by electron microscopy," *Nature* **257**, 28–32 (1975).
10. K. M. Al-Aribe, G. K. Knopf, and A. S. Bassi, "Ionic polymer microactuator activated by photoresponsive organic proton pumps," *Actuators* **4**, 237–254 (2015).
11. A. Maeda, T. Iwasa, and T. Yoshizawa, "Isomeric composition of retinal chromophore in dark-adapted bacteriorhodopsin," *J. Biochem.* **82**(6), 1599–1604 (1977).
12. F. Gai et al., "Chemical dynamics in proteins: the photoisomerization of retinal in bacteriorhodopsin," *Science* **279**, 1886–1891 (1988).
13. J. K. Lanyi, "Proton translocation mechanism and energetics in the light-driven pump bacteriorhodopsin," *Biochim. Biophys. Acta* **1183**, 241–261 (1993).
14. G. Váró and L. Keszthelyi, "Photoelectric signals from dried oriented purple membranes of Halobacterium halobium," *Biophys. J.* **43**, 47–51 (1983).

15. R. Korenstein and B. Hess, "Hydration effects on cis-trans isomerization of bacteriorhodopsin," *FEBS Lett.* **82**, 7–11 (1977).
16. Y. Cao et al., "Water is required for proton transfer from aspartate-96 to the bacteriorhodopsin Schiff base," *Biochemistry* **30**, 10972–10979 (1991).
17. G. I. Groma et al., "Photocycle of dried acid purple form of bacteriorhodopsin," *Biophys. J.* **81**, 3432–3441 (2001).
18. W. W. Wang, G. K. Knopf, and A. S. Bassi, "Time and frequency response characteristics of bacteriorhodopsin-based photodetectors," *Opt. Eng.* **45**, 084001 (2006).
19. W. W. Wang, G. K. Knopf, and A. S. Bassi, "Protein-based photoreceptor array on flexible plastic substrates," in *Smart Biosensor Technology*, G. K. Knopf and A. S. Bassi, Eds., pp. 461–502, CRC Press, Boca Raton, Florida (2007).
20. K. Ludmann, C. Gergely, and G. Váró, "Kinetic and thermodynamic study of the bacteriorhodopsin photocycle over a wide pH range," *Biophys. J.* **75**, 3110–3119 (1998).
21. Z. Dancshazy et al., "The photochemical cycle of bacteriorhodopsin has no refractory period," *FEBS Lett.* **196**(2), 198–202 (1986).
22. C. Ganea et al., "The role of water in the extracellular half channel of bacteriorhodopsin," *Biophys. J.* **73**, 2718–2725 (1997).
23. R. Henderson et al., "Model for the structure of bacteriorhodopsin based on high-resolution electron cryomicroscopy," *J. Mol. Biol.* **213**, 899–929 (1990).
24. E. M. Landau and J. P. Rosenbusch, "Lipidic cubic phases: a novel concept for the crystallization of membrane proteins," *Proc. Natl. Acad. Sci. U. S. A.* **93**, 14532–14535 (1996).
25. A. Roy et al., "Helix deformation is coupled to vectorial proton transport in the photocycle of bacteriorhodopsin," *Nature* **406**, 645–648 (2000).
26. S. Subramaniam and R. Henderson, "Molecular mechanism of vectorial proton translocation by bacteriorhodopsin," *Nature* **406**, 653–657 (2000).
27. H. Luecke et al., "Structure of bacteriorhodopsin at 1.55 A resolution," *J. Mol. Biol.* **291**(4), 899–911 (1999).
28. F. T. Hong, "Interfacial photochemistry of retinal proteins," *Prog. Surf. Sci.* **62**, 1–237 (1999).
29. R. R. Birge et al., "Biomolecular electronics: protein-based associative processors and volumetric memories," *J. Phys. Chem. B* **103**, 10746–10766 (1999).
30. S. Y. Liu, "Light-induced currents from oriented purple membrane I. Correlation of the microsecond component (B2) with the L-M photocycle transition," *Biophys. J.* **57**, 943–950 (1990).
31. W. W. Wang, G. K. Knopf, and A. S. Bassi, "Spherical imaging array based on bioelectronic photoreceptors," *Proc. SPIE* **6375**, 63750K (2006).
32. J. A. He et al., "Bacteriorhodopsin thin film assemblies: immobilization, properties, and applications," *Adv. Mater.* **11**, 435–446 (1999).
33. K. M. Al-Aribe, G. K. Knopf, and A. S. Bassi, "Photoelectric monolayers based on self-assembled and oriented purple membrane patches," *J. Microelectromech. Syst.* **20**(4), 800–810 (2011).
34. M. Schranz, F. Noll, and N. Hampp, "Oriented purple membrane monolayers covalently attached to gold by multiple thiole linkages analyzed by single molecule force spectroscopy," *Langmuir* **23**(22), 11134–11138 (2007).
35. K. Koyama, N. Yamaguchi, and T. Miyasaka, "Antibody-mediated bacteriorhodopsin orientation for molecular device architectures," *Science* **265**(5173), 762–765 (1994).
36. R. Henderson, J. Stubb, and S. Whytock, "Specific labelling of the protein and lipid on the extracellular surface of purple membrane," *J. Mol. Biol.* **123**, 259–274 (1978).
37. D. Chen et al., "Oriented assembly of purple membrane on solid support mediated by molecular recognition," *J. Phys. Chem. B* **107**(15), 3598–3605 (2003).
38. Q. Ren et al., "A nanomechanical device based on light-driven proton pumps," *Nanotechnology* **17**(6), 1778–1785 (2006).

39. I. M. Pepe and C. Nicolini, "Langmuir–Blodgett films of photosensitive proteins," *J. Photochem. Photobiol. B* **33**(3), 191–200 (1996).
40. J. Xu, P. Bhattacharya, and G. Váró, "Monolithically integrated bacteriorhodopsin/semiconductor opto-electronic integrated circuit for a bio-photoreceiver," *Biosens. Bioelectron.* **19**, 885–892 (2004).
41. A. Dér, P. Hargittai, and J. Simon, "Time-resolved photoelectric and absorption signals from oriented purple membranes immobilized in gel," *J. Biochem. Biophys. Methods* **10**(5–6), 259–300 (1985).
42. J. Xu, "Bio-photosensors based on monolithic integration of light sensitive proteins with semiconductor devices and integrated circuits," PhD Dissertation, University of Michigan-Ann Arbor, Department of Electrical Engineering and Computer Science (2003).
43. L. Zhang et al., "High performance photovoltaic behavior of oriented purple membrane polymer composite films," *Biophys. J.* **84**, 2502–2507 (2003).
44. N. Yamaguchi et al., "Visualization of the morphology of purple membrane surfaces by monoclonal antibody techniques," *FEBS Lett.* **324**, 287–292 (1993).
45. J. Gau et al., "A MEMS based amperometric detector for E. coli bacteria using self-assembled monolayers," *Biosens. Bioelectron.* **16**(9–12), 745–755 (2001).
46. L. Gervais et al., "Immobilization of biotinylated bacteriophages on biosensor surfaces," *Sens. Actuators B Chem.* **125**(2), 615–621 (2007).
47. P. S. Stayton et al., "Streptavidin assemblies that communicate," in *Protein Architecture: Interfacing Molecular Assemblies and Immobilization Biotechnology*, Y. Lvov and H. Moehwald, Eds., pp. 287–309, Marcel Dekker, New York (1999).
48. R. H. Tredgold, *Order in Thin Organic Films*, Cambridge University Press, Cambridge, United Kingdom (1994).
49. A. P. Gast et al., "Two-dimensional streptavidin crystals: macropatterns and microorganization," *Biomol. Eng.* **16**, 21–27 (1999).
50. C. Horn and C. Steinem, "Photocurrents generated by bacteriorhodopsin adsorbed on nanoblack lipid membranes," *Biophys. J.* **89**(2), 1046–1054 (2005).
51. C.-W. Chang et al., "Fabrication and photovoltaic characterization of biosensitized solar cells using mygobin-based sensitizers," *J. Nanotechnol.* **8**, 1–8 (2008).
52. M. Grätzel, "Solar energy conversion by dye-sensitized photovoltaic cell," *Inorg. Chem.* **44**(20), 6841–6851 (2005).
53. B. O'Regan and M. Grätzel, "A low-cost, high-efficiency solar cell based on dye sensitized colloidal TiO_2 films," *Nature* **353**, 737–740 (1991).
54. K. Wongcharee, V. Meeyoo, and S. Chavadej, "Dye-sensitized solar cell using natural dyes extracted from rosella and blue pea flowers," *Sol. Energy Mater. Sol. Cells* **91**(7), 566–571 (2007).
55. R. Das et al., "Integration of photosynthetic protein molecular complexes in solid-state electronic devices," *Nano Lett.* **4**(6), 1079–1083 (2004).
56. D. Ho et al., "Fabrication of biomolecule-copolymer hybrid nanovesicles as energy conversion systems," *Nanotechnology* **16**, 3120 (2005).
57. T. Miyasaka, K. Koyama, and I. Itoh, "Quantum conversion and image detection by a bacteriorhodopsin-based artificial photoreceptor," *Science* **255**, 342–344 (1992).
58. T. Yagishita et al., "Effects of glucose addition and light on current outputs in photosynthetic electrochemical cells using Synechocystis sp. PCC671," *J. Biosci. Bioeng.* **88**(2), 210–214 (1999).
59. W. W. Wang, G. K. Knopf, and A. S. Bassi, "Bioelectronic imaging array based on bacteriorhodopsin film," *IEEE Trans. Nanobiosci.* **7**, 249–256 (2008).
60. L. Lensu et al., "Photoelectric properties of bacteriorhodopsin analogs for color-sensitive optoelectronic devices," *Opt. Mater.* **27**, 57–62 (2004).

61. S. Roy et al., "All-optical switching with bacteriorhodopsin protein coated microcavities and its application to low power computing circuits," *J. Appl. Phys.* **107**, 053115 (2010).
62. K. Al-Aribe and G. K. Knopf, "Photoresponsive hydrogel microvalve activated by bacteriorhodopsin proton pumps," *Proc. SPIE* **7646**, 764611 (2010).
63. K. A. Walczak et al., "Electronic characteristics of bacteriorhodopsin," in *Proc. of 8th IEEE Conf. Nanotechnology*, pp. 553–556 (2008).
64. W. W. Wang, "Bioelectronic photocell and flexible photoreceptor array based on bacteriorhodopsin film," PhD Dissertation, University of Western Ontario, Department of Mechanical and Materials Engineering (2006).
65. U. Alexiev et al., "Surface charge of bacteriorhodopsin detected with covalently bound pH indicators at selected extracellular and cytoplasmic sites," *Biochemistry* **33**, 298–306 (1994).
66. W. W. Wang, G. K. Knopf, and A. S. Bassi, "Biological transducers based on bacteriorhodopsin for smart biosensor applications," in *Proc. 2004 Int. Conf. on MEMS, NANO and Smart Systems (ICMENS '04)*, pp. 243–248 (2004).
67. M. Ahmadi and J. T. W. Yeow, "Fabrication and characterization of a radiation sensor based on bacteriorhodopsin," *Biosens. Bioelectron.* **26**, 2171–2176 (2011).
68. A. Dolfi, G. Aloisi, and R. Guidelli, "Photoelectric response of purple membrane fragments adsorbed on a lipid monolayer supported by mercury and characterization of the resulting interphase," *Bioelectrochemistry* **57**, 155–166 (2002).
69. S. Liu and T. Ebrey, "Photocurrent measurements of the purple membrane oriented in polyacrylamide gel," *Biophys. J.* **54**, 321–329 (1988).
70. R. R. Birge, "Protein-based computers," *Sci. Am.* **272**(3), 90–95 (1995).
71. C. P. Collier et al., "Electronically configurable molecular-based logic gates," *Science* **285**, 391–394 (1999).
72. F. T. Hong, "Photoelectric biosensors: fundamentals and innovative designs," in *Smart Biosensor Technology*, G. K. Knopf and A. S. Bassi, Eds., CRC Press (2007).
73. G. Rayfield, "Ultra high speed bacteriorhodopsin photodetectors," in *Molecular Electronics Biosensors and Biocomputers*, F. T. Hong, Ed., pp. 361–368, Plenum Press, New York (1989).
74. J. Min et al., "Visual information processing using bacteriorhodopsin-based complex LB films," *Biosens. Bioelectron.* **16**(9–12), 917–923 (2001).
75. T. Miyasaka and K. Koyama, "Image sensing and processing by a bacteriorhodopsin-based artificial photoreceptor," *Appl. Opt.* **32**(31), 6371–6379 (1993).
76. J. Yang and G. Wang, "Image edge detecting by using the bacteriorhodopsin-based artificial ganglion cell receptive field," *Thin Solid Films* **324**, 281–284 (1998).
77. K. Fukuzawa, "Motion-sensitive position sensor using bacteriorhodopsin," *Appl. Opt.* **33**(31), 7489–7495 (1994).
78. L. Lensu et al., "Color-sensitive biosensors for imaging applications," in *Smart Biosensor Technology*, G. Knopf and A. Bassi, Eds., CRC Press/Taylor & Francis, Boca Raton, Florida (2007).
79. M. Frydrych et al., "Color sensitive retina based on bacteriorhodopsin," *Biosystems* **54**, 131–140 (2000).
80. K. J. Vahala, "Optical microcavities," *Nature* **424**, 839–846 (2003).
81. J. Topolancik and F. Vollmer, "All-optical switching in the near infrared with bacteriorhodopsin-coated microcavities," *Appl. Phys. Lett.* **89**, 184103 (2006).
82. J. Topolancik and F. Vollmer, "Photoinduced transformations in bacteriorhodopsin membrane monitored with optical microcavities," *Biophys. J.* **92**, 2223–2229 (2007).
83. S. Roy et al., "All-optical reversible logic gates with optically controlled bacteriorhodopsin protein-coated microresonators," *Adv. Opt. Technol.* **2012**, 727206 (2012).

84. P. Ormos et al., "Protein-based integrated optical switching and modulation," *Appl. Phys. Lett.* **80**(21), 4060–4062 (2002).
85. Y. Huang, S.-T. Wu, and Y. Zhao, "Photonic switching based on the photoinduced birefringence in bacteriorhodopsin films," *Appl. Phys. Lett.* **84**(12), 2028–2030 (2004).
86. P. Wu et al., "Enhancement of photoinduced anisotropy and all-optical switching in bacteriorhodopsin films," *Appl. Phys. Lett.* **81**(20), 3888–3890 (2002).
87. C. J. G. Kirkby and I. Bennion, "Organic photochromics for spatial light modulation," *IEE Proc. J: Optoelectron.* **133**, 98–104 (1986).
88. Y. Saga et al., "Mechanism of photocurrent generation from bacteriorhodopsin on gold electrodes," *J. Phys. Chem. B* **103**(1), 234–238 (1999).
89. D. Haronian and A. Lewis, "Microfabricating bacteriorhodopsin films for imaging and computing," *Appl. Phys. Lett.* **61**, 2237–2239 (1992).
90. J. A. Stuart et al., "Bacteriorhodopsin: from biophotonic material to chemical sensor," in *Smart Biosensor Technology*, G. K. Knopf and A. S. Bassi, Eds., CRC Press/Taylor & Francis, Boca Raton, Florida (2007).
91. C. H. Martin, Z. P. Chen, and R. R. Birge, "Towards a bacteriorhodopsin-silicon neuromorphic photosensor," in *Proc. Pacific Symp. on Biocomputing*, pp. 268–279 (1997).
92. S. Libertino et al., "Characterization and patterning of bacteriorhodopsin films on Si-based materials," *Synth. Met.* **138**, 71–74 (2003).
93. A. A. Kononenko et al., "Oriented purple membrane films as a probe for studies of the mechanism of bacteriorhodopsin functioning. I. The vectorial character of the external electric-field effect on the dark state and the photocycle of bacteriorhodopsin," *Biochim. Biophys. Acta* **850**, 162–169 (1986).
94. W. Reichardt, "Autocorrelation, a principle for evaluation of sensory information by the central nervous system," in *Sensory Communication*, pp. 303–317, MIT Press, Cambridge, Massachusetts (1961).
95. A. Sangole and G. K. Knopf, "Representing high-dimensional data sets as close surfaces," *J. Inf. Visualization* **1**(1), 111–119 (2002).
96. S. Haykin, *Neural Networks A Comprehensive Foundation*, Prentice Hall, Upper Saddle River, New Jersey (1999).
97. J. Suzurikawa et al., "Microscale pH gradient generation by electrolysis on a light-addressable planar electrode," *Sens. Actuators B* **149**, 205–211 (2010).
98. T. M. Pabst and G. Carta, "Separation of protein charge variants with induced pH gradients using anion exchange chromatographic columns," *Biotechnol. Prog.* **24**, 1096–1106 (2008).
99. X. Cheng et al., "An electrochemical fabrication process for the assembly of anisotropically oriented collagen bundles," *Biomaterials* **29**, 3278–3288 (2008).
100. K. M. Al-Aribe, G. K. Knopf, and A. S. Bassi, "Fabrication of an optically driven pH gradient generator based on self-assembled proton pumps," *Microfluid. Nanofluid.* **12**(1–4), 325–335 (2012).
101. R. H. Liu, Q. Yu, and D. Beebe, "Fabrication and characterization of hydrogel-based microvalves," *J. Microelectromech. Syst.* **11**(1), 45–53 (2002).
102. A. Baldi et al., "A hydrogel-actuated environmentally sensitive microvalve for active flow control," *J. Microelectromech. Syst.* **12**(5), 613–621 (2003).
103. T. Watanabe et al., "Photoresonsive hydrogel microstructure fabricated by two-photon initiated polymerization," *Adv. Funct. Mater.* **12**, 611–614 (2002).
104. N. A. Peppas et al., "Hydrogels in biology and medicine: from molecular principles to bionanotechnology," *Adv. Mater.* **18**, 1345–1360 (2006).
105. S. R. Sershen et al., "Independent optical control of microfluidic valves formed from optomechanically responsive nanocomposite hydrogels," *Adv. Mater.* **17**, 1366–1368 (2005).

106. I. Eroglu et al., "Photoresponse of bacteriorhodopsin immobilized in polyacrylamide gel membranes," *J. Membr. Sci.* **86**, 171–179 (1994).
107. K. Al-Aribe, G. K. Knopf, and A. S. Bassi, "Photo-responsive hydrogel for controlling flow on a microfluidic chip," *Proc. SPIE* **6343**, 63432R (2006).
108. E. C. Achilleos et al., "Quantifying deformation in gel swelling: experiments and simulations," *Am. Inst. Chem. Eng.* **46**(11), 2128–2139 (2000).
109. C.-C. Lin and A. T. Metters, "Hydrogels in controlled release formulations: network design and mathematical modeling," *Adv. Drug Delivery Rev.* **58**, 1379–1408 (2006).
110. Y. Chiu et al., "pH-induced swelling kinetics of polyelectrolyte hydrogels," *J. Appl. Polym. Sci.* **58**, 2161–2176 (1995).
111. A. Richter et al., "Review on hydrogel-based pH sensors and microsensors," *Sensors* **8**, 561–581 (2008).
112. J. Jang et al., "Three dimensionally-patterned submicrometer-scale hydrogel/air networks that offer a new platform for biomedical applications," *Nano Lett.* **8**, 1456–1460 (2008).

George K. Knopf is a Professor in the Department of Mechanical and Materials Engineering at the University of Western Ontario, Canada. His research interests include bioelectronics, biosensors, and laser materials processing. Current activities include the development of conductive graphene-based inks and novel fabrication processes for printing electronic circuitry on mechanically flexible surfaces. Dr. Knopf has co-edited two CRC Press volumes entitled Smart Biosensor Technology and Optical Nano and Micro Actuator Technology.

Khaled M. Al-Aribe received his B.S. and M.S. degrees in Mechanical Engineering from the University of Garyounis, Benghazi, Libya, in 1992 and 1999, respectively, and Ph.D. degrees in Mechanical and Materials Engineering from the University of Western Ontario, London, ON, Canada in 2012. He is an Assistant Professor in the Department of Mechanical Engineering, Abu Dhabi University, Abu Dhabi, UAE. His research activities involve smart materials, biomaterials, photo-responsive films, self-assembled monolayers, and piezoelectric films.